# Benemérita Universidad Autónoma de Puebla

## Facultad de Ciencias Físico Matemáticas

Testing the Change of Flavour in the production of Higgs bosons at the LHeC and the LHC.

Tesis presentada al

**Posgrado de Física**

como requisito parcial para la obtención del grado de

**Doctor en Ciencias (Física Aplicada)**

por

Sebastián Rosado Navarro

asesorado por

Dr. Jaime Hernández Sánchez

Puebla Pue.
Marzo de 2020

**Título:** Testing the Change of Flavour in the production of Higgs bosons at the LHeC and the LHC.
**Estudiante:**Sebastián Rosado Navarro

COMITÉ

Dr. Justiniano Lorenzo Díaz Cruz
Presidente

Dr. Humberto Salazar Ibargüen
Secretario

Dra. María Isabel Pedraza Morales
Vocal

Dr. Jaime Hernández Sánchez
Asesor

# Contents

# Aknowledgements

Este trabajo es dedicado a todos aquellos que me han apoyado en mi formación como físico a lo largo de estos años.

A mi madre, Dra. Reyla Areli Navarro Cruz, quien siempre me ha ofrecido su amor y apoyo en las buenas y en las malas. Gracias por todos estos años.

A mi padre, Dr. Alfonso Rosado Sánchez, quien también ha ofrecido amor y apoyo y sin querer me inspiró a estudiar esta interesante carrera. Valoro mucho todo el apoyo que me brindó al estudiar esta carrera, incluso aunque yo por necio intentara no tomarlo.

A mi pareja, Karla Aydeé Ramírez Hernández, mi musa y compañera, quien me ha enseñado conocimientos ajenos a mi área y se ha interesado tanto por lo que he trabajado. Gracias a ella he crecido más como persona y siempre tendrá un lugar muy especial en mi corazón.

A mi asesor el Dr. Jaime Hernández Sánchez por su invaluable amistad, apoyo, ideas y paciencia.

Al Profesor Stefano Moretti por la amistad, todo el apoyo brindado durante mi estancia en la Universidad de Southampton en Reino Unido y la Universidad de Carleton, Ottawa en Canadá.

A la Profesora Heather Logan por recibirme en la Universidad de Carleton, Ottawa y por su invaluable aporte al trabajo realizado.

Al Dr. Justiniano Lorenzo Díaz Cruz por sus conversaciones tan interesantes de física y sugerencias para la realización de esta tesis.

Al Dr. Arturo Fernández Téllez, quien me brindó mucho apoyo a lo largo de varios años.

A todos aquellos físicos que me preceden, espero llegar a estar a la altura de poder ser considerado uno de ustedes.

# Abstract

In this thesis work, we study the production of a lightly charged Higgs boson at the future Large Hadron electron Collider (LHeC), through the process $ep \to \nu_e H^{\pm} q^{'}$ considering both channel decays $H^{\pm} \to cb$ and $H^{\pm} \to \tau\nu_{\tau}$, and at the Large Hadron Collider (LHC) through the quark fussion process $q_1 q_2 \to \tau\nu_{\tau}$ with the decay mode $H^{\pm} \to \tau\nu_{\tau}$. These processes are analysed in the context of the Two Higgs Doublet Model type III (2HDM-III).

# Introduction

The discovery of a 125 $GeV$ resonance in proton-proton ($pp$) collisions at the Large Hadron Collider (LHC) [4], which is likely to correspond to be the Standard Model (SM) Higgs boson. The SM of strong and electroweak interactions describes in a very precise way the elementary particles physics at the energies available at current colliders. The Higgs scalar sector, one of the main concepts of the model, can be considered proven. In the SM, the Higgs sector contains a complex scalar Higgs doublet, and after the spontaneous symmetry breaking, there is a remnant in the form of a physical state, the scalar Higgs boson ($h^0_{sm}$). Nevertheless, because of many reasons, many particle physicists consider, that the SM Higgs sector is not the ultimate theoretical structure that explains the electroweak symmetry breaking. [63, 64].

The SM has achieved great success after years of its conception. Impressive results have been obtained for the the neutral $Z^0$ and the charged $W^{\pm}$ bosons parameters, as well as the *top* quark mass, among others. The evidence of the Higgs boson existence was the last missing piece of the SM. The Higgs boson plays a very important role in the explanation of the elementary particles mass origin, particularly the difference between the massless photon and the massive gauge bosons $W^{\pm}$ and $Z^0$. The fundamental massive particles and the difference between the electromagnetic interactions, mediated through photons, and the weak force, mediated through the $W^{\pm}$ and $Z^0$ gauge bosons, are critical in many aspects of the subatomic structure of matter. Now that it is known that there is a boson with many properties similar to those of the Higgs boson, the remaining question is: could it be the lightest scalar of a more complex Higgs sector than the one from the SM [63]? The great scale difference between forces, the existence of three particle families, the mass difference between them, among other phenomena, led to the development of extensions of the SM. Some of the models are supersymmetry, extra dimensions, technicolour, string theory, etc.

One of the simplest SM extensions are the Two Higgs Doublet Model (2HDM) [45]. This models includes a Higgs sector with two scalar doublets, which give mass to the *up* and *down* type fermions under several flavour mechanisms on the couplings, while also giving mass to the gauge bosons. A $Z_2$ symmetry might be added, thus the model might be constructed into three different forms:

- Type-I: This one is mostly used for models with dark matter.
- Type-II: In this case, one Higgs scalar doublet couples to the *up* components of the fermionic isodoublets, while the other Higgs scalar doublet couples to the *down* components and the leptons. The 2HDM-II is mostly used in supersymmetrical theories.
- Type-III: This is the most general model and might not have a $Z_2$ symmetry [53].

The 2HDM-II has a rich structure and predicts interesting phenomenology [63]. The psysical spectre consists of two neutral CP-even states ($h^0, H^0$) and one CP-odd ($A^0$), as well as couple of two charged scalar particles ($H^{\pm}$). The advantage of 2HDM is the fact that any Higgs sector built only with doublets naturally preserves the lowest order in $\alpha$ the $\rho$ electroweak relation, where $\rho = M^2_{W^{\pm}}/(M^2_Z \cos^2\theta)$, which has been proven with great precision. From a phenomenological point of view, an important aspect of the 2HDM is that the Higgs sector can provide an additional source of violation of CP [75, 74, 95, 97, 76]. A source of CP violation is searched since in nature this phenomenon has been seen, in the decays from kaons to pions [46].

The present thesis work is organized as follows: in the Chapter 1, a revision on SM is presented; in Chapter 2 the 2HDM is reviewed; in chapter 3 the $H^{\pm}$ production at the LHeC is studied profoundly; in chapter 4 the $H^{\pm}$ production at the LHeC through quark fusion process and decay into $\tau\nu\tau$ is studied.

# Chapter 1

# Standard Model

## 1.1 Overview

The Standard Model (SM) is a Quantum Field Theory, which describes the physics of elementary particles and their interactions. The experiments have proven its predictions with great precision [67, 79, 72, 57, 96]. The elementary particles are considered to be two types in the SM, the structure of matter, and the mediators of the interactions. The first ones are $s = \frac{1}{2}$ fermions: the quarks and the leptons [12, 61, 84].

The known leptons are the electron $e^-$, the muon $\mu^-$ and the tauon $\tau^-$ with electric charge $Q = -1|e|$ (all charges are given in units of the fundamental electric charge $e$), and their corresponding neutrinos $\nu_e$, $\nu_\mu$ and $\nu_\tau$ with charge $Q = 0$. The known quarks are of six different flavours, the up quarks: $u$, $c$ and $t$ with electric charge $Q = \frac{2}{3}|e|$; the down quarks: $d$, $s$ and $b$ with electric charge $Q = -\frac{1}{3}|e|$.

The quarks have an additional quantum number, the colour, which can be of three types, denoted generically as $q_i$, $(i = 1, 2, 3)$. Since colour is not observed in nature, quarks must be confined in "colourless" material particles called hadrons. These composite particles are classified into baryons and mesons. Baryons are fermions composed of three quarks, $qqq$, such as the proton, $p \sim uud$ and the neutron, $n \sim udd$. The mesons are bosons formed by a quark and an antiquark, $q\overline{q}$, such as the pions, $\pi^+ \sim u\overline{d}$, and $\pi^- \sim \overline{u}d$.

The second class of fundamental particles are the intermediate particles of the interactions. The relevant interactions in particle physics [1] are mediated by the exchange of a fundamental particle that is a spin boson $s = 1$. The photon, $\gamma$, is the particle that mediates electromagnetic interactions; the eight gluons $g_\alpha$ $(\alpha = 1, ..., 8)$ mediate the strong interactions between the quarks, and the three massive bosons, $W^\pm$ and $Z^0$ are the corresponding intermediate vector bosons of the weak interactions.

The SM is based on the gauge symmetry $SU(3)_C \times SU(2)_L \times U(1)_Y$, and this is why it is known as a gauge theory. This gauge group includes the symmetry group of the strong interactions, $SU(3)_C$ [54, 29, 30], and the symmetry group of the electroweak interactions, $SU(2)_L \times U(1)_Y$ [48, 59, 82]. The symmetry group of the electromagnetic interactions, $U(1)_{em}$, appears in the SM as a subset of $SU(2)_L \times U(1)_Y$ and in this sense it is said that weak and electromagnetic interactions are unified.

For the study of particles and their interactions in the model, three sectors are defined:

- The fermionic sector
- The standard bosonic sector
- The scalar sector or sector of Higgs.

### 1.1.1 Fermionic Sector

The quarks and leptons are organized into three families (see Table 1.1). Each family contains two flavours of quarks ($u^i$, $i$; where $i$ indicates the colour charge) and two of leptons (neutrinos $\nu_l$ and leptons

[1] Gravitational interaction is not relevant at low energies. The gravitational interactions are mediated by the hypothetical particle called graviton, which has spin $s = 2$.

$l$ electron type). These families have identical properties, with the exception of the mass. The content of particles in each family is shown in Table 1.1; besides these, they have their corresponding antiparticles. The left and right fields are defined by the chirality operator $\gamma^5$ as:

$$e_L^- = \frac{1}{2}\left(1-\gamma_5\right)e^-, \quad e_R^- = \frac{1}{2}\left(1+\gamma_5\right)e^-, \tag{1.1}$$

and the transform as $SU(2)_L$ doublets and singlets, respectively.

| | | | | | |
|---|---|---|---|---|---|
| First family: | $\begin{pmatrix} \nu_e \\ e^- \end{pmatrix}_L$, | $e_R^-$, | $\begin{pmatrix} u \\ d \end{pmatrix}_L$, | $u_R$, | $d_R$, |
| Second family: | $\begin{pmatrix} \nu_\mu \\ \mu^- \end{pmatrix}_L$, | $\mu_R^-$, | $\begin{pmatrix} c \\ s \end{pmatrix}_L$, | $c_R$, | $s_R$, |
| Third family: | $\begin{pmatrix} \nu_\tau \\ \tau^- \end{pmatrix}_L$, | $\tau_R^-$, | $\begin{pmatrix} t \\ b \end{pmatrix}_L$, | $t_R$, | $b_R$. |

Table 1.1: SM quark and lepton families.

### 1.1.2 Gauge Sector

This sector is composed of eight gluons, which are the gauge bosons of $SU(3)_C$ and the particles $W^\pm$, $Z^0$ and $\gamma$ which are the four gauge bosons of $SU(2)_L \times U(1)_Y$. The main physical properties of these intermediate gauge bosons are: the gluons have zero mass, are electrically neutral and have colour charge, which can be of eight different types [61]. As a result of this, gluons interact not only with quarks, but also with themselves. The bosons $W^\pm$ and $Z^0$ are massive particles, therefore they have a limited interaction range. Due to the $U(1)$ group being Abelian, there are no self interaction within phtons, on the other hand the $SU(2)_L$ and $SU(3)_C$ are not Abelian groups, therefore self interactions appear. The $W^\pm$ bosons have an electrical charge $Q = \pm 1|e|$, respectively, while the $Z^0$ is electrically neutral. The $\gamma$ is electrically neutral, massless, thus the interaction range is infinite, and does not interact with itself.

To ensure the left helicity fermions couplings with the gauge boson $W^\pm$, fermions of this type are represented by doublets of $SU(2)_L$,

$$Q_L = \begin{pmatrix} U \\ D \end{pmatrix}_L \quad L_L = \begin{pmatrix} N \\ E \end{pmatrix}_L,$$

where $Q_L$ and $L_L$ are quark and lepton doublets in $SU(2)_L$, respectively. The right helicity fermion states are transformed as singlets under $SU(2)_L$; but both, quarks and leptons, doublets and singlets, are transformed non-trivially under the hypercharge group $U(1)_Y$. For the fermions, the quantum numbers $Q$, $T_3$, and $Y$ are defined, which are the electric charge, the weak charge and the hypercharge, respectively. The values of these quantum numbers are shown in Table 1.2 for the fermionic states in the SM.

| Quantum numbers | $U_R$ | $U_L$ | $D_R$ | $D_L$ | $N_L$ | $E_R$ | $E_L$ |
|---|---|---|---|---|---|---|---|
| $Y$ | 2/3 | 1/6 | -1/3 | 1/6 | -1/2 | -1 | -1/2 |
| $T_3$ | 0 | 1/2 | 0 | -1/2 | 1/2 | 0 | -1/2 |
| $Q$ | 2/3 | 2/3 | -1/3 | -1/3 | 0 | -1 | -1 |

Table 1.2: Quantum numbers associated to fermions within the SM, in the case of $Q$, in $e\pm$ units.

### 1.1.3 Scalar Sector

The fact that the weak gauge bosons are massive, implies that $SU(2)_L \times U(1)_Y$ is not a vacuum symmetry. Thus, a Higgs doublet is included to generate the mass of the electroweak bosons $W^\pm$ and $Z^0$ [68, 69, 38, 28, 39], as well as the fermions (except the neutrinos), this is due to the terms of mass

$$M_W^2 W_a^\mu W_\mu^a \quad o \quad m\overline{\psi}\psi = m(\psi_L\psi_R + \psi_R\psi_L), \tag{1.2}$$

when introduced directly, destroy the invariance of norm $SU(2)_L \times U(1)_Y$, and therefore the renormalizability of the theory. To avoid this problem, the best known solution is to include in the SM the Higgs sector, which induces a spontaneous break of the symmetry, that is,

$$SU(3)_C \times SU(2)_L \times U(1)_Y \longrightarrow SU(3)_C \times U(1)_{em}. \tag{1.3}$$

This is done through the so-called Higgs Mechanism, which provides the correct masses to the standard bosons $W^{\pm}$ and $Z^0$ and to the fermions, and leaves as a consequence the prediction of a new particle: the Higgs Boson.

On the other hand, one of the problems that has not been clarified in the SM, is to know the representation of the Higgs boson that perhaps will manifest in future experiments. This is because the Higgs mechanism is not unique, and there are many representations of Higgs bosons that correctly describe the dynamics of the spontaneous break of electroweak symmetry.

However, the minimum version includes a complex scalar doublet under $SU(2)_L$ given by

$$\Phi = \begin{pmatrix} \phi^+ \\ \phi^0 \end{pmatrix} ,$$

which is a singlet under the group $SU(3)_C$, with an associated hypercharge $Y_\Phi = 1$, and with weak isospin $T = 1/2$.

## 1.2 The Higgs Mechanism

One of the key points of the SM of electroweak interactions is the concept of Spontaneous Symmetry Breaking (SSB), which results in the appearance of Goldstone excitations [58], which are related to mass terms of the standard bosons. When the SSB refers to a standard symmetry instead of a global one, then it is the Higgs mechanism that operates.

In the SM, the symmetry breaking is carried out by a scalar field, which acquires a vacuum expectation value (v.e.v.) different from zero. The resulting physical spectrum contains not only the massive gauge bosons and the fermionic fields, but also the Higgs particle, an electrically neutral scalar field.

### 1.2.1 Spontaneous Symmetry Breaking

In the framework of quantum field theory it is said that a system has a spontaneously broken symmetry, if the Lagrangian that describes the dynamics of the system is invariant under these symmetry transformations, but the vacuum of the theory does not. Here the vacuum, $|0\rangle$, is the state in which the expectation value of the Hamiltonian $\langle 0|\mathbf{H}|0\rangle$ is minimal.

One of the physical implications of the SSB phenomenon is the appearance of non-massive modes. The general situation in quantum field theory is described by Goldstone's theorem [58, 59]: If the Lagrangian of a theory has a global symmetry, which is not a vacuum symmetry, then there must be a non-massive, scalar or pseudoscalar boson associated with each generator that does not annihilate the vacuum and has the same quantum numbers.

These modes are known as Nambu-Goldstone bosons or simply Goldstone bosons. Goldstone's theorem is for theories with spontaneous breaks of global symmetries, but loses its validity for gauge theories. In this case it is the Higgs mechanism that operates [58, 59]: The Goldstone-type bosons associated with global spontaneous symmetry breaking do not manifest explicitly in the physical spectrum, but "combine" with non-massive standard bosons and as a result, once the spectrum of the theory it is built on the asymmetric vacuum, massive vector particles appear. The number of vector bosons that acquire mass is precisely the number of Goldstone bosons.

### 1.2.2 Symmetry Breaking Sector

Let $\Phi$ be the system that provides the breaking $SU(2)_L \times U(1)_Y \to U(1)_{em}$ . Then $\Phi$ must meet the following requirements:

- Must be a scalar field so that the SSB preserves the Lorentz invariance.

- Must be a complex field so that the Hamiltonian is hermitian.
- Must have values of hypercharge and weak isospin different from zero in order to break $SU(2)_L$ and $U(1)_Y$.
- Only the $\Phi$ neutral components will acquire nonzero v.e.v. nonzero so that the $U(1)_{em}$ symmetry of the vacuum is preserved.
- The $\Phi$ interactions with the fermionic and gauge sectors must be gauge invariant.
- The $\Phi$ self-interactions given by the potential $V(\Phi)$ must produce the desired break, which is characterized in this case by

$$\langle 0|\Phi^\dagger\Phi|0\rangle \neq 0.$$

- $V(\Phi)$ must be renormalizable.

Taking these points into account, the simplest choice for the $\Phi$ system and the Lagrangian of the symmetry breaking sector of the electroweak theory is:

$$\mathcal{L}_{SB} = \left(\mathcal{D}_\mu\Phi\right)^\dagger\left(\mathcal{D}^\mu\Phi\right) - V\left(\Phi\right), \tag{1.4}$$

$$V(\Phi) = -\mu^2\Phi^\dagger\Phi + \lambda\left(\Phi^\dagger\Phi\right)^2 \quad \text{con} \quad \lambda > 0\,, \tag{1.5}$$

where

$$\Phi = \begin{pmatrix} \phi^+ \\ \phi^0 \end{pmatrix} = \frac{1}{\sqrt{2}}\begin{pmatrix} \phi_1 + i\phi_2 \\ \phi_3 + i\phi_4 \end{pmatrix}, \tag{1.6}$$

$$\mathcal{D}_\mu\Phi = \left(\partial_\mu - ig\frac{\tau^j}{2}W_\mu^j - i\frac{g'}{2}B_\mu\right)\Phi\,. \tag{1.7}$$

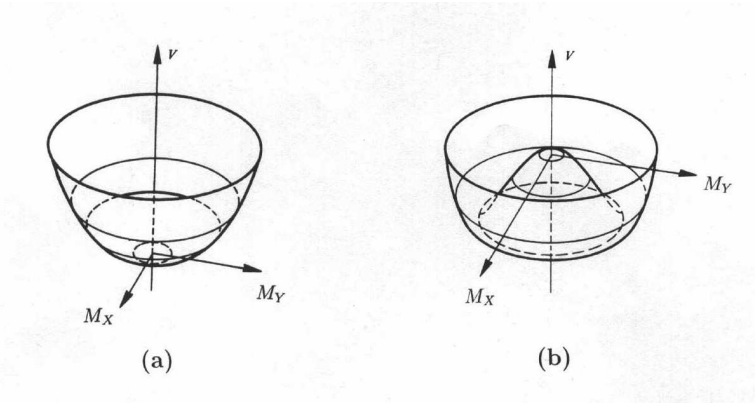


Figure 1.1: The $V(\Phi)$ potential in the symmetric phase and the SSB phase.

Here, $\Phi$ is a fundamental complex doublet, $\tau^j$ is the isospin operators; $g$ and $g'$ are the gauge coupling constants corresponding to the groups $SU(2)_L$ and $U(1)_Y$, respectively; $W_\mu^j$ and $B_\mu$ are the gauge fields of $SU(2)_L$ and $U(1)_Y$, respectively. Depending on the sign of the mass parameter $(-\mu^2)$, there are two possible v.e.v. $\langle 0|\Phi^\dagger\Phi|0\rangle$ minimizing the potential $V(\Phi)$:

1. $(-\mu^2) > 0$: the minimum is

$$\langle 0|\Phi^\dagger\Phi|0\rangle = 0\,, \tag{1.8}$$

then the vacuum has symmetry $SU(2)_L \times U(1)_Y$ and therefore there is no symmetry breaking, which is represented graphically in Fig. 1.1(a).

2. $(-\mu^2) < 0$: the minimum is

$$|\langle 0|\Phi^\dagger\Phi|0\rangle| = -\frac{\mu^2}{\lambda}\,, \tag{1.9}$$

therefore there is an infinite number of degenerate vacua corresponding to the infinite number of possible values for $\langle 0|\Phi^\dagger\Phi|0\rangle$, so

$$\Phi^2 = \Phi^\dagger\Phi = \frac{1}{2}(\phi_1^2+\phi_2^2+\phi_3^2+\phi_4^2) = -\frac{\mu^2}{\lambda}\ .$$

Any of these vacua has symmetry $U(1)_{em}$ but not $SU(2)_L{\times}U(1)_Y$. The $SU(2)_L{\times}U(1)_Y \longrightarrow U(1)_{em}$ break occurs once a particular vacuum is chosen, graphically shown in Fig. 1.1 (b). The simplest possibility can be taken, without loss of generality:

$$\begin{aligned} &\langle\phi_1^2\rangle_0 = -\tfrac{\mu^2}{\lambda}\,; \quad \langle\phi_2^2\rangle_0 = \langle\phi_3^2\rangle_0 = \langle\phi_4^2\rangle_0 = 0\,; \\ &|\langle 0|\Phi^\dagger\Phi|0\rangle| = \begin{pmatrix} 0 \\ \frac{v}{\sqrt{2}} \end{pmatrix}; \qquad v^2 \equiv -\frac{\mu^2}{\lambda} \end{aligned} \tag{1.10}$$

Another interesting aspect of the Higgs mechanism is that it preserves the number of degrees of polarization. These are:

- Before the SSB: There is a complex scalar doublet $\Phi$ (with $4\times 1 = 4$ degrees of freedom), the non-massive gauge fields $W^j$ (with $3\times 2 = 6$ degrees of freedom), and the non-massive gauge field $B$ (with $1\times 2 = 2$ degrees of freedom), for a total of 12 degrees of freedom.
- After the SSB: There is a real physical scalar $h^0_{SM}$ (with $1\times 1 = 1$ degree of freedom), the massive fields $W^\pm$ and $Z^0$ (with $3\times 3 = 9$ degrees of freedom), and a non-massive $\gamma$ photon (with $1\times 2 = 2$ degrees of freedom), for a total of 12 degrees of freedom.

It is said that scalar degrees of freedom have been " eaten " to give the standard bosons $W^\pm$ and $Z^0$ their longitudinal components. It is important to notice that an extra degree of freedom was introduced from the beginning into the theory to those needed. Three of the actual components of $\Phi$, $\phi^\pm \equiv \frac{1}{\sqrt{2}}(\phi_1 \mp i\phi_2)$ and $\chi = \phi_3$, are the Goldstone bosons needed in the theory and the fourth $\phi_4$ is introduced only to complete the complex doublet.

After the symmetry breaking, this extra degree of freedom results in the appearance of a massive scalar particle in the spectrum, the Higgs boson $h^0_{SM}$.

### 1.2.3 Particle Masses

In order to obtain the particles spectra and their masses it is first needed to write the Lagrangian of the SM, which is $SU(2)_L \times U(1)_Y$ gauge invariant:

$$\mathcal{L}_{SM} = \mathcal{L}_f + \mathcal{L}_G + \mathcal{L}_{SB} + \mathcal{L}_{YW}\,, \tag{1.11}$$

where the $\mathcal{L}_f$ is the Lagrangian for the fermionic sector, $\mathcal{L}_G$ is for the gauge bosonic sector, $\mathcal{L}_{SB}$ is the one for the symmetry breaking sector and $\mathcal{L}_{YW}$ is the Yukawa Lagrangian, which are given by:

$$\mathcal{L}_f = \sum_{f=l,q} \overline{f} i\not{\mathcal{D}} f\,, \tag{1.12}$$

$$\mathcal{L}_G = -\frac{1}{4}W^i_{\mu\nu}W_i^{\mu\nu} - \frac{1}{4}B_{\mu\nu}B^{\mu\nu} + \mathcal{L}_{GF} + \mathcal{L}_{FP}\,, \tag{1.13}$$

$$\mathcal{L}_{SB} = \left(\mathcal{D}_\mu\Phi\right)^\dagger\left(\mathcal{D}^\mu\Phi\right) + \mu^2\Phi^\dagger\Phi - \lambda\left(\Phi^\dagger\Phi\right)^2\,, \tag{1.14}$$

$$\mathcal{L}_{YW} = \lambda_e\overline{l}_L\Phi e_R + \lambda_u\overline{q}_L\widetilde{\Phi}u_R + \lambda_d\overline{q}_L\Phi d_R + h.c.\,, \tag{1.15}$$

in these expressions,

$$W^i_{\mu\nu} = \partial_\mu W^i_\nu - \partial_\nu W^i_\mu + g\epsilon^{ijk}W^j_\mu W^k_\nu\,, \tag{1.16}$$

$$B_{\mu\nu} = \partial_\mu B_\nu - \partial_\nu B_\mu \,, \tag{1.17}$$

$$\begin{aligned} l_L &= \begin{pmatrix} \nu_L \\ e_L \end{pmatrix}, \quad q_L = \begin{pmatrix} u_L \\ d_L \end{pmatrix}, \\ \Phi &= \begin{pmatrix} \phi^+ \\ \phi^0 \end{pmatrix}, \quad \widetilde{\Phi} = \begin{pmatrix} \phi_0^* \\ -\phi^- \end{pmatrix}. \end{aligned} \tag{1.18}$$

$\mathcal{L}_{GF}$ and $\mathcal{L}_{FP}$ are the gauge correction and Faddeev-Popov Lagrangians, respectively, which are necessary in any gauge theory. Note that the Lagrangian $\mathcal{L}_{SB}$ is needed to provide the masses $M_{W^\pm}$ and $M_{Z^0}$, while $\mathcal{L}_{YW}$ provides the masses $M_f$.

The procedure to obtain the spectrum from $\mathcal{L}_{SM}$ is as follows:

1. A non-symmertic vacuum must be fixed, so (1.10) is chosen,

$$|\langle 0|\Phi^\dagger \Phi|0\rangle| = \begin{pmatrix} 0 \\ \frac{\upsilon}{\sqrt{2}} \end{pmatrix}. \tag{1.19}$$

2. The physical spectrum is build doing "small oscillations" around this vacuum. This small oscillations are parametrized by

$$\Phi(x) = \exp\left(i\frac{\overline{\xi}(x)\cdot\overline{\sigma}}{\upsilon}\right)\begin{pmatrix} 0 \\ \frac{\upsilon+h^\circ_{SM}(x)}{\sqrt{2}} \end{pmatrix}, \tag{1.20}$$

   where $\overline{\xi}(x)$ and $h^\circ_{SM}(x)$ are "small" fields.

3. In order to eliminate the non-physical fields $\overline{\xi}(x)$ the following gauge transformations are made:

$$\begin{gathered} U(\xi) = \exp\left(-i\tfrac{\overline{\xi}\cdot\overline{\sigma}}{\upsilon}\right); \qquad \Phi' = U(\xi)\Phi = \begin{pmatrix} 0 \\ \frac{\upsilon+h^\circ_{SM}(x)}{\sqrt{2}} \end{pmatrix}; \\ l'_L = U(\xi) l_L; \qquad e'_R = e_R; \\ q'_L = U(\xi) q_L; \qquad u'_R = u_R; \qquad d'_R = d_R; \\ B'_\mu = B_\mu; \\ \left(\tfrac{\overline{\sigma}\cdot\overline{W}'_\mu}{2}\right) = U(\xi)\left(\tfrac{\overline{\sigma}\cdot\overline{W}_\mu}{2}\right)U^{-1}(\xi) - \tfrac{i}{g}\left(\partial_\mu U(\xi)\right)U^{-1}(\xi)\,. \end{gathered} \tag{1.21}$$

4. Finally, the weak eigenstates are rotated into the mass eigenstates, which define the physical gauge bosonic fields:

$$W^\pm_\mu = \frac{W'^1_\mu \mp i W'^2_\mu}{\sqrt{2}}, \tag{1.22}$$

$$Z_\mu = W'^3_\mu \cos\theta_W - B'_\mu \sin\theta_W, \tag{1.23}$$

$$A_\mu = W'^3_\mu \sin\theta_W + B'_\mu \cos\theta_W\,. \tag{1.24}$$

Now it is possible to obtain the physical particle masses from the following $\mathcal{L}_{SM}$ terms:

$$\left(\mathcal{D}_\mu\Phi'\right)^\dagger\left(\mathcal{D}^\mu\Phi'\right) = \left(\frac{g^2\upsilon^2}{4}\right)W^+_\mu W^{\mu-} + \frac{1}{2}\left(\frac{\left(g^2+g'^2\right)\upsilon^2}{4}\right)Z_\mu Z^\mu + \dots\,, \tag{1.25}$$

$$V\left(\Phi'\right) = \frac{1}{2}\left(2\mu^2\right)h^{\circ 2}_{SM} + \dots\,, \tag{1.26}$$

$$\mathcal{L}_{YW} = \left(\lambda_e\frac{\upsilon}{\sqrt{2}}\right)\overline{e}'_L e'_R + \left(\lambda_u\frac{\upsilon}{\sqrt{2}}\right)\overline{u}'_L u'_R + \left(\lambda_d\frac{\upsilon}{\sqrt{2}}\right)\overline{d}'_L d'_R + \dots\,. \tag{1.27}$$

Finally, it is obtained the tree-level predictions:

$$\begin{aligned} &M_{W^\pm} = \frac{g\upsilon}{2}\,; \quad M_{Z^0} = \frac{\sqrt{(g^2+g'^2)}\upsilon}{2}\,; \qquad M_\gamma = 0\,; \\ &m_e = \lambda_e \frac{\upsilon}{\sqrt{2}}\,; \qquad m_u = \lambda_u \frac{\upsilon}{\sqrt{2}}\,; \qquad m_d = \lambda_d \frac{\upsilon}{\sqrt{2}}\,; \ldots\,, \\ &\qquad\qquad \text{y} \\ &\qquad\qquad M_{h^\circ_{SM}} = \sqrt{2}\mu\,, \end{aligned} \tag{1.28}$$

where

$$\upsilon = \sqrt{-\frac{\mu^2}{\lambda}}\,. \tag{1.29}$$

With this $\mathcal{L}_{SB}$ and $\mathcal{L}_{YW}$ can be rewritten, after applying the Higgs mechanism, in terms of the physical scalar fields, and obtain not only the mass terms, but also the interaction and kinetic terms in the Higgs sector,

$$\mathcal{L}_{SB} + \mathcal{L}_{YW} \to \mathcal{L}^{free}_{h^\circ_{SM}} + \mathcal{L}^{int}_{h^\circ_{SM}} + \ldots \tag{1.30}$$

where

$$\mathcal{L}^{free}_{h^\circ_{SM}} = \frac{1}{2}\partial_\mu h^\circ_{SM}\partial^\mu h^\circ_{SM} - \frac{1}{2}M^2_{h^\circ_{SM}} h^{\circ 2}_{SM} \tag{1.31}$$

$$\begin{aligned} \mathcal{L}^{int}_{h^\circ_{SM}} \;=\; & -\frac{M^2_{h^\circ_{SM}}}{\upsilon^2} h^{\circ 3}_{SM} - \frac{M^2_{h^\circ_{SM}}}{8\upsilon^2} h^{\circ 4}_{SM} - \frac{m_e}{\upsilon}\overline{f} h^\circ_{SM} f \\ & + M^2_W W^+_\mu W^{\mu -}\left(1 + \frac{2}{\upsilon}h^\circ_{SM} + \frac{2}{\upsilon^2}h^{\circ 2}_{SM}\right) \\ & + M^2_Z Z_\mu Z^\mu\left(1 + \frac{2}{\upsilon}h^\circ_{SM} + \frac{2}{\upsilon^2}h^{\circ 2}_{SM}\right) \end{aligned} \tag{1.32}$$

Now, all the masses are given in terms of a single mass parameter $\upsilon$ and of the couplings $g$, $g'$, $\lambda$, $\lambda_e$, etc. Likewise, the the Higgs boson interactions $h^0_{SM}$ with the fermions and the gauge bosons are proportional to the gauge couplings and to the corresponding particle masses:

$$\begin{aligned} f\overline{f}h^\circ_{SM} \;&:\; -i\frac{g}{2}\frac{m_f}{M_W}; \\ W^+_\mu W^-_\nu h^\circ_{SM} \;&:\; igM_W g_{\mu\nu}; \\ Z_\mu Z_\nu h^\circ_{SM} \;&:\; i\frac{g}{\cos\theta_W}M_Z g_{\mu\nu}. \end{aligned} \tag{1.33}$$

Experimentally it has been found that [79]:

$$M_{W^\pm} = 80.425 \pm 0.038 \text{ GeV}\,,$$

$$M_Z = 91.1876 \pm 0.0021 \text{ GeV}\,.$$

Using these values,

$$\upsilon = 254 \text{ GeV}.$$

From equation (1.28) it can be seen that

$$\frac{M_W}{M_Z} = \frac{g}{\sqrt{g^2+g'^2}} = \cos\theta_W\,. \tag{1.34}$$

Since the bosons $Z^0$ and $W^{\pm}$ are not degenerate in mass (unless $\theta_W \to 0$), once measured $\theta_W$, the result of the equation (1.34) is a prediction of the SM, which has turned out to be consistent with the experiments.

A useful quantity to consider is

$$\rho \equiv \frac{M_W}{M_Z \cos\theta_W}\,, \tag{1.35}$$

which is worth 1 for the SM [2]. Any deviation of $\rho_{SM} = 1$ is a sign of the existence of a new physics.

[2] In fact, it has been shown that even if there are additional Higgs doublets, the parameter $\rho_{SM} = 1$ does not change [63].

# Chapter 2

# Two Higgs Doublets Model

The 2HDM scalar sector has very interesting characteristics. In its most general form, it is possible to have fourteen interpendent parameters [53]. However, the fact that the Higgs doublets $\Phi_1$ and $\Phi_2$ are not physically observable (only the mass eigenstates are physical particles) means that there is the freedom to redefine these doublets, as long as the shape of its kinetic terms are kept. These base changes of Higgs doublets allow us to absorb some of the parameters in the potential and are essential to understand the number of physical parameters present in it [53].

It is common to impose global symmetries on the 2HDM, in order to reduce the number of free parameters [55]. The symmetries have different effects on the potential and, therefore, different physical implications: different spectra of the scalars, interactions between gauge bosons and in certain cases predictions of non-massive axions or candidates for dark matter[40].

The vacuum is defined in the 2HDM potential and this, unlike the one obtained in the SM, is not unique. With two Higgs doublets, the vacuum can spontaneously break the CP symmetry. On the other hand, for certain values of the parameters in the potential there are vacua that can violate the electromagnetic symmetry, thus giving mass to the photon. These should be avoided. Even if it is considered only the vacua that preserve CP and the gauge symmetries of the SM, the 2HDM has a significant vacuum structure: some of the possible potentials for the 2HDM can present "inert vacuum", in which one of the neutral scalars does not fit gauge bosons and can also be decoupled from fermions in a simple way [94].

Not all parameter values in the 2HDM potential ensure that there is a stable minimum, unless it can be assured that it is bounded below. The basic requirement allows restrictions to be placed on quartic scalar couplings. An improvement in the renormalization group of these constraints results in restrictive limits in the masses of the physical scalar particles.

## 2.1 General 2HDM potential

Let us define the fields of the two Higgs doublets as

$$\Phi_1 = \begin{pmatrix} \phi_1^+ \\ \frac{\phi_{1\mathbb{R}}^0 + i\phi_{1\Im}^0 + v_1}{\sqrt{2}} \end{pmatrix} \quad \text{y} \quad \Phi_2 = \begin{pmatrix} \phi_2^+ \\ \frac{\phi_{2\mathbb{R}}^0 + i\phi_{2\Im}^0 + v_2}{\sqrt{2}} \end{pmatrix} , \tag{2.1}$$

where $\phi^{\pm} \in \mathbb{C}$ and is such that $(\phi^{\pm})^* = \phi^{\mp}$. In this way the vacuum expectation values of expectation in the vacuum are real and therefore there is no spontaneous breaking of CP.

For the most general renormalizable scalar potential the following notation shall be used

$$\begin{aligned} V_{Gen} &= -m_{11}^2\Phi_1^\dagger\Phi_1 - m_{22}^2\Phi_2^\dagger\Phi_2 - (m_{12}^2\Phi_1^\dagger\Phi_2 + \text{h.c.}) \\ &+ \frac{1}{2}\lambda_1(\Phi_1^\dagger\Phi_1)^2 + \frac{1}{2}\lambda_2(\Phi_2^\dagger\Phi_2)^2 + \frac{1}{2}\lambda_3(\Phi_1^\dagger\Phi_1)(\Phi_2^\dagger\Phi_2) + \frac{1}{2}\lambda_4(\Phi_1^\dagger\Phi_2)(\Phi_2^\dagger\Phi_1) \\ &+ [\frac{1}{2}\lambda_5(\Phi_1^\dagger\Phi_2)^2 + \lambda_6(\Phi_1^\dagger\Phi_1)(\Phi_1^\dagger\Phi_2) + \lambda_7(\Phi_2^\dagger\Phi_2)(\Phi_1^\dagger\Phi_2) + \text{h.c.}], \end{aligned} \tag{2.2}$$

where "h.c." means Hermitian conjugate. The parameters $m_{11}^2$, $m_{22}^2$ and $\lambda_{1,2,3,4}$ are real. In general, $m_{12}^2$ and $\lambda_{5,6,7}$ are complex. Therefore, the potential depends on six real and four complex parameters, giving a total of fourteen degrees of freedom.

A problem with this model is the appearance of flavour change through neutral currents (FCNC) due to the terms $\lambda_6$ and $\lambda_7$. This problem can be avoided by adding four-zero texture mass matrices to the Yukawa sector [66].

## 2.2 2HDM with $Z_2$ symmetry

The discrete symmetry $Z_2$ is defined as $\Phi_1 \to \Phi_1$, $\Phi_2 \to -\Phi_2$, and for the fermions $d \to d$ and $u \to -u$. In this way it is guaranteed the absence FCNC [56]. With this discrete symmetry it is obtained two types of 2HDM, but in both cases it can be started from the same potential, in which $\lambda_{6,7} = 0$ to preserve the symmetry, but this can be broken softly (see the term $m_{12}^2$). Thus, the potential that strictly conserves $Z_2$ has the form

$$\begin{aligned} V_{Z_2} &= -m_{11}^2\Phi_1^\dagger\Phi_1 - m_{22}^2\Phi_2^\dagger\Phi_2 \\ &+ \frac{1}{2}\lambda_1(\Phi_1^\dagger\Phi_1)^2 + \frac{1}{2}\lambda_2(\Phi_2^\dagger\Phi_2)^2 + \frac{1}{2}\lambda_3(\Phi_1^\dagger\Phi_1)(\Phi_2^\dagger\Phi_2) + \frac{1}{2}\lambda_4(\Phi_1^\dagger\Phi_2)(\Phi_2^\dagger\Phi_1) \\ &+ [\frac{1}{2}\lambda_5(\Phi_1^\dagger\Phi_2)^2 + \text{h.c.}], \end{aligned} \tag{2.3}$$

and the one that has a symmetry $Z_2$ soft breaking,

$$\begin{aligned} V_{Z_2Soft} &= m_{11}^2\Phi_1^\dagger\Phi_1 + m_{22}^2\Phi_2^\dagger\Phi_2 - (m_{12}^2\Phi_1^\dagger\Phi_2 + \text{h.c.}) \\ &+ \frac{1}{2}\lambda_1(\Phi_1^\dagger\Phi_1)^2 + \frac{1}{2}\lambda_2(\Phi_2^\dagger\Phi_2)^2 + \frac{1}{2}\lambda_3(\Phi_1^\dagger\Phi_1)(\Phi_2^\dagger\Phi_2) + \frac{1}{2}\lambda_4(\Phi_1^\dagger\Phi_2)(\Phi_2^\dagger\Phi_1) \\ &+ [\frac{1}{2}\lambda_5(\Phi_1^\dagger\Phi_2)^2 + \text{h.c.}]. \end{aligned} \tag{2.4}$$

## 2.3 Spontaneous Charge Conservation Breaking

If one of the doublets is defined in the following way

$$\Phi_2 = \begin{pmatrix} \phi_2^+ + u \\ \frac{\phi_{2\Re}^0 + i\phi_{2\Im}^0 + v_2}{\sqrt{2}} \end{pmatrix}, \tag{2.5}$$

so that $u$ is real, a charge violation at the tree level in the potential is acquired. For not having no such break, then $u = 0$. [42]

## 2.4 CP Conservation

To preserve the discrete CP symmetry, $m_{12}^2$ and $\lambda_{5,6,7}$ have to be real, and that the doublets have the form of the equation (2.1).

## 2.5 Minimalization conditions and diagonalized mass matrices

The necessary calculations to obtain the mass matrices for the 2HDM-III will be performed, for this first the minimalization conditions have to be found. Taking the results it can be started the symmetry models $Z_2$ without problems, simply certain terms will disappear depending on whether the model is type-I or type-II.

Starting with the minimization conditions. For this the next choice is made

$$\langle \Phi_1 \rangle = \begin{pmatrix} 0 \\ \frac{v_1}{\sqrt{2}} \end{pmatrix} \text{ and } \langle \Phi_2 \rangle = \begin{pmatrix} 0 \\ \frac{v_2}{\sqrt{2}} \end{pmatrix}, \tag{2.6}$$

so it is obtain that

$$\begin{aligned} m_{11}^2 &= -\frac{1}{2}\left( v_1^2\lambda_1 + v_2^2\lambda_{345} + \frac{v_2\left(3v_1^2\lambda_6 + v_2^2\lambda_7\right)}{v_1} - \frac{2m_{12}^2 v_2}{v_1} \right), \\ m_{22}^2 &= -\frac{1}{2}\left( v_2^2\lambda_2 + v_1^2\lambda_{345} + \frac{v_1\left(v_1^2\lambda_6 + 3v_2^2\lambda_7\right)}{v_1} - \frac{2m_{12}^2 v_1}{v_2} \right), \\ \lambda_{345} &= \lambda_3 + \lambda_4 + \lambda_5, \end{aligned} \tag{2.7}$$

Having the minimization conditions, the mass matrix by calculations of the expression is calculated

$$M_{ij}^2 = \frac{\partial^2 V(\Phi_1, \Phi_2)}{\partial\phi_i \partial\phi_j}. \tag{2.8}$$

The resulting matrix can be separated in the charged sector and the neutral one. In this case there will be 3 matrices of $2 \times 2$, one for the sector with load and the other two for the real part and the imaginary part of the neutral sector. Then the following matrices are acquired:

$$\begin{aligned} M_{H^\pm}^2 &= \begin{pmatrix} \frac{m_{12}^2 v_2}{v_1} - \frac{v_2^2(\lambda_4+\lambda_5)}{2} - \frac{\lambda_6 v_1 v_2}{2} - \frac{\lambda_7 v_2^3}{2v_1} & -m_{12}^2 + \frac{v_1 v_2(\lambda_4+\lambda_5)}{2} + \frac{v_1^2\lambda_6}{2} + \frac{v_2^2\lambda_7}{2} \\ -m_{12}^2 + \frac{v_1 v_2(\lambda_4+\lambda_5)}{2} + \frac{v_1^2\lambda_6}{2} + \frac{v_2^2\lambda_7}{2} & -\frac{\lambda_6 v_1^3}{2v_2} - \frac{(\lambda_4+\lambda_5)v_1^2}{2} - \frac{v_1 v_2\lambda_7}{2} + \frac{m_{12}^2 v_1}{v_2} \end{pmatrix}, \\ M_A^2 &= \begin{pmatrix} \frac{m_{12}^2 v_2}{v_1} - \lambda_5 v_2^2 - \frac{v_1 v_2\lambda_6}{2} - \frac{\lambda_7 {v_2}^3}{2v_1} & -m_{12}^2 + v_1 v_2\lambda_5 + \frac{v_1^2\lambda_6}{2} + \frac{v_2^2\lambda_7}{2} \\ -m_{12}^2 + v_1 v_2\lambda_5 + \frac{v_1^2\lambda_6}{2} + \frac{v_2^2\lambda_7}{2} & \frac{m_{12}^2 v_1}{v_2} - \lambda_5 v_1^2 - \frac{\lambda_6 {v_1}^3}{2v_3} - \frac{v_1 v_2\lambda_7}{2} \end{pmatrix}, \\ M_{H,h} &= \begin{pmatrix} \frac{m_{12}^2 v_2}{v_1} + v_1^2\lambda_1 + \frac{3v_1 v_2\lambda_6}{2} - \frac{\lambda_7 v_2^3}{2v_1} & -m_{12}^2 + v_1 v_2\lambda_{345} + \frac{3v_1^2\lambda_6}{2} + \frac{3v_2^2\lambda_7}{2} \\ -m_{12}^2 + v_1 v_2\lambda_{345} + \frac{3v_1^2\lambda_6}{2} + \frac{3v_2^2\lambda_7}{2} & \frac{m_{12}^2 v_1}{v_2} + v_2^2\lambda_2 - \frac{\lambda_6 v_1^3}{2v_2} + \frac{3v_1 v_2\lambda_7}{2} \end{pmatrix}. \end{aligned} \tag{2.9}$$

To simplify the calculation of the real neutral matrix, its entries are as follows

$$M_{H,h} = \begin{pmatrix} \mu_{11}^2 & \mu_{12}^2 \\ \mu_{12}^2 & \mu_{22}^2 \end{pmatrix}.$$

Diagonalizing the matrices (2.9), the eigenestates of the masses are

$$m_A^2 = \frac{m_{12}^2 v^2}{v_1 v_2} - v^2\lambda_5 - \frac{v^2 v_1\lambda_6}{2v_2} - \frac{v^2 v_2\lambda_7}{2v_1}, \tag{2.10}$$

$$m_{H^\pm}^2 = m_A + \frac{v^2(\lambda_5 - \lambda_4)}{2}, \tag{2.11}$$

$$m_{H,h}^2 = \frac{1}{2}\left( {\mu_{11}}^2 + {\mu_{22}}^2 - \sqrt{{\mu_{11}}^4 + 4{\mu_{12}}^4 - 2{\mu_{11}}^2{\mu_{22}}^2 + {\mu_{22}}^4} \right), \tag{2.12}$$

where $v^2 = v_1^2 + v_2^2$

## 2.6 Brief 2HDM Summary

- 2HDM type-I: In this model, a doublet is decoupled from the Yukawa sector, that is, the other doublet is coupled in a manner very similar to that of the SM. The difference lies in the potential, which in this case may be that one of the vacuum expectation values is zero, this will cause the symmetry $Z_2$ not even break softly. The case in which both values are different from zero will be developed for the type-II model.

- 2HDM type-II: The supersymmetric minimum standard model uses this model for its spontaneous break of gauge symmetry. In this case, one of the doublets will be coupled to the "down " and lepton type fermions while the other to the "up" types. This case has the soft symmetry break $Z_2$. The fact that the doublets are coupled according to the type of fermion is what, unlike the type-I model, makes each doublet have a vacuum expectation value.

- 2HDM type-III: The 2HDM type-III uses the most general scalar potential. This type of model mainly affects the Yukawa sector, which will be studied later. In short, this type of model implies that the two Higgs doublets will be attached to all the fermions. In this case there could be no symmetry $Z_2$. In this model, both doublets will have vacuum expectation values. As a particular case of this potential, there can be conservation of the symmetry $Z_2$ in the quartic terms, that is, when $\lambda_{6,7} = 0$.

## 2.7 The Yukawa Sector in the 2HDM-III with a four-zero texture

In this section, the main model for this thesis work is revisited, and relies heavily on [66]. In Ref. [43], a specific four-zero texture has been implemented for the Yukawa matrices within the 2HDM-III. This allows one to express the couplings of the neutral and charged Higgs bosons in terms of the fermion masses, Cabibbo-Kobayashi-Maskawa (CKM) mixing angles and certain dimensionless parameters, which are to be bounded by current experimental constraints. Thus, in order to derive the interactions of the charged Higgs boson, the Yukawa Lagrangian is written as follows:

$$\begin{aligned}\mathcal{L}_Y \quad &= -\Big(Y_1^u \bar{Q}_L \tilde{\Phi}_1 u_R + Y_2^u \bar{Q}_L \tilde{\Phi}_2 u_R + Y_1^d \bar{Q}_L \Phi_1 d_R \\ &\quad + Y_2^d \bar{Q}_L \Phi_2 d_R + Y_1^l \bar{L_L} \Phi_1 l_R + Y_2^l \bar{L_L} \Phi_2 l_R\Big), \end{aligned} \tag{2.13}$$

where $\Phi_{1,2} = (\phi^+_{1,2}, \phi^0_{1,2})^T$ refer to the two Higgs doublets, $\tilde{\Phi}_{1,2} = i\sigma_2 \Phi^*_{1,2}$, $Q_L$ denotes the left-handed fermion doublet, $u_R$ and $d_R$ are the right-handed fermion singlets and, finally, $Y^{u,d}_{1,2}$ denote the $(3 \times 3)$ Yukawa matrices. Similarly, one can see the corresponding left-handed fermion doublet $L_L$, the right-handed fermion singlet $l_R$ and the Yukawa matrices $Y^l_{1,2}$ for leptons.

After spontaneous EW Symmetry Breaking (EWSB), one can derive the fermion mass matrices from eq. (2.13), namely

$$M_f = \frac{1}{\sqrt{2}}(v_1 Y_1^f + v_2 Y_2^f), \qquad f = u, d, l. \tag{2.14}$$

It will be assumed that both Yukawa matrices $Y_1^f$ and $Y_2^f$ have the four-texture form and are Hermitian [51, 43]. Following this convention, the fermions mass matrices have the same form, which can be written as:

$$M_f = \begin{pmatrix} 0 & C_f & 0 \\ C_f^* & \tilde{B}_f & B_f \\ 0 & B_f^* & A_f \end{pmatrix}. \tag{2.15}$$

When $\tilde{B}_q \to 0$ one recovers the six-texture form. It is also considered the hierarchy $\mid A_q \mid \gg \mid \tilde{B}_q \mid, \mid B_q \mid, \mid C_q \mid$, which is supported by the observed fermion masses in the SM.

The mass matrix is diagonalized through the bi-unitary matrices $V_{L,R}$, though each Yukawa matrices is not diagonalized by this transformation. The diagonalization is performed in the following way:

$$\bar{M}_f = V_{fL}^\dagger M_f V_{fR}. \tag{2.16}$$

The fact that $M_f$ is Hermitian, under the considerations given above, directly implies that $V_{fL} = V_{fR}$, and the mass eigenstates for the fermions are given by

$$u = V_u^\dagger u', \qquad d = V_d^\dagger d', \qquad l = V_l^\dagger l'. \tag{2.17}$$

Then, eq. (2.14) in this basis takes the form

$$\bar{M}_f = \frac{1}{\sqrt{2}}(v_1 \tilde{Y}_1^f + v_2 \tilde{Y}_2^f), \tag{2.18}$$

where $\tilde{Y}_i^f = V_{fL}^\dagger Y_i^f V_{fR}$. In order to compare the kind of new physics coming from the Yukawa texture with some more traditional 2HDMs (in particular with the 2HDM-II), in previous works [43, 41, 22, 60, 65], some of us have adopted the following re-definitions:
2HDM-II-like

$$\begin{aligned}
\tilde{Y}_1^d &= \frac{\sqrt{2}}{v\cos\beta}\bar{M}_d - \tan\beta \tilde{Y}_2^d, \\
\tilde{Y}_2^u &= \frac{\sqrt{2}}{v\sin\beta}\bar{M}_u - \cot\beta \tilde{Y}_1^u, \\
\tilde{Y}_1^l &= \tilde{Y}_1^d (d \to l).
\end{aligned} \tag{2.19}$$

These re-definitions are convenient because the Higgs-fermion-fermion coupling in the 2HDM-III can be $g^{ff\phi}_{\rm 2HDM-III} = g^{ff\phi}_{\rm 2HDM-II} + \Delta g^{ff\phi}$, where $g^{ff\phi}_{\rm 2HDM-II}$ is the coupling in the 2HDM-II and $\Delta g^{ff\phi}$ is the contribution of the four-zero texture. If $\Delta g^{ff\phi} \to 0$ the 2HDM-II can recovered. However, these re-definitions are not unique. In fact, there are others possibilities since from eq. (2.18) one can reproduce the 2HDM-I, 2HDM-X or 2HDM-Y as one can obtain for any version of 2HDM the following relation: $g^{ff\phi}_{\rm 2HDM-III} = g^{ff\phi}_{\rm 2HDM-any} + \Delta' g^{ff\phi}$. The other possible re-definitions are:
2HDM-I-like

$$\begin{aligned}
\tilde{Y}_2^d &= \frac{\sqrt{2}}{v\sin\beta}\bar{M}_d - \cot\beta \tilde{Y}_1^d, \\
\tilde{Y}_2^u &= \frac{\sqrt{2}}{v\sin\beta}\bar{M}_u - \cot\beta \tilde{Y}_1^u, \\
\tilde{Y}_2^l &= \tilde{Y}_2^d (d \to l).
\end{aligned} \tag{2.20}$$

2HDM-X-like

$$\begin{aligned}
\tilde{Y}_2^d &= \frac{\sqrt{2}}{v\sin\beta}\bar{M}_d - \cot\beta \tilde{Y}_1^d, \\
\tilde{Y}_2^u &= \frac{\sqrt{2}}{v\sin\beta}\bar{M}_u - \cot\beta \tilde{Y}_1^u, \\
\tilde{Y}_1^l &= \tilde{Y}_1^d (d \to l).
\end{aligned} \tag{2.21}$$

2HDM-Y-like

$$\begin{aligned}
\tilde{Y}_1^d &= \frac{\sqrt{2}}{v\cos\beta}\bar{M}_d - \tan\beta \tilde{Y}_2^d, \\
\tilde{Y}_2^u &= \frac{\sqrt{2}}{v\sin\beta}\bar{M}_u - \cot\beta \tilde{Y}_1^u, \\
\tilde{Y}_2^l &= \tilde{Y}_2^d (d \to l).
\end{aligned} \tag{2.22}$$

After spontaneous EWSB and including the diagonalizing matrices for quarks and Higgs bosons[1], the interactions of the charged Higgs bosons $H^\pm$ and neutral Higgs bosons $\phi^0$ ($\phi^0 = h^0$, $H^0$, $A^0$ ) with quark pairs for any

[1]The details of both diagonalizations are presented in Ref. [43].

parametrization 2HDM-(I,II,X,Y)-like have the following form:

$$
\begin{aligned}
\mathcal{L}^{\bar{f}_i f_j \phi} &= -\frac{g}{2\sqrt{2}M_W}\Bigg[\sum_{l=1}^{3}\bar{u}_i\Bigg\{(V_{\rm CKM})_{il}\left[X\, m_{d_l}\,\delta_{lj} - f(X)\left(\frac{\sqrt{2}M_W}{g}\right)\left(\tilde{Y}^{d}_{n(X)}\right)_{lj}\right](1+\gamma^5) \\
&+\left[Y\, m_{u_i}\,\delta_{il} - f(Y)\left(\frac{\sqrt{2}M_W}{g}\right)\left(\tilde{Y}^{u}_{n(Y)}\right)^{\dagger}_{il}\right](V_{\rm CKM})_{lj}(1-\gamma^5)\Bigg\}\, d_j\, H^+ \\
&+\bar{\nu}_i\left[Z\, m_{l_i}\,\delta_{ij} - f(Z)\left(\frac{\sqrt{2}M_W}{g}\right)\left(\tilde{Y}^{l}_{n(Z)}\right)_{ij}\right](1+\gamma^5) l_j H^+ + h.c.\Bigg] \\
&-\frac{g}{2M_W}\Bigg(m_{d_i}\bar{d}_i\Bigg\{\left[\xi^d_H\delta_{ij} - \frac{(\xi^d_h + X\xi^d_H)}{f(X)}\frac{\sqrt{2}}{g}\left(\frac{m_W}{m_{d_i}}\right)(\tilde{Y}^{d}_{n(X)})_{ij}\right]H^0 \\
&+\left[\xi^d_h\delta_{ij} + \frac{(\xi^d_H - X\xi^d_h)}{f(X)}\frac{\sqrt{2}}{g}\left(\frac{m_W}{m_{d_i}}\right)(\tilde{Y}^{d}_{n(X)})_{ij}\right]h^0 \\
&+i\left[-X\delta_{ij} + f(X)\frac{\sqrt{2}}{g}\left(\frac{m_W}{m_{d_i}}\right)(\tilde{Y}^{d}_{n(X)})_{ij}\right]\gamma^5 A^0\Bigg\} d_j \\
&+m_{u_i}\bar{u}_i\Bigg\{\left[\xi^u_H\delta_{ij} + \frac{(\xi^u_h - Y\xi^u_H)}{f(Y)}\frac{\sqrt{2}}{g}\left(\frac{m_W}{m_{u_i}}\right)(\tilde{Y}^{u}_{n(Y)})_{ij}\right]H^0 \\
&+\left[\xi^u_h\delta_{ij} - \frac{(\xi^u_H + Y\xi^u_h)}{f(Y)}\frac{\sqrt{2}}{g}\left(\frac{m_W}{m_{u_i}}\right)(\tilde{Y}^{u}_{n(Y)})_{ij}\right]h^0 \\
&+i\left[-Y\delta_{ij} + f(Y)\frac{\sqrt{2}}{g}\left(\frac{m_W}{m_{u_i}}\right)(\tilde{Y}^{u}_{n(Y)})_{ij}\right]\gamma^5 A^0\Bigg\} u_j \\
&+m_{l_i}\bar{l}_i\Bigg\{\left[\xi^l_H\delta_{ij} - \frac{(\xi^l_h + Z\xi^l_H)}{f(Z)}\frac{\sqrt{2}}{g}\left(\frac{m_W}{m_{d_i}}\right)(\tilde{Y}^{l}_{n(Z)})_{ij}\right]H^0 \\
&+\left[\xi^l_h f(Z)\delta_{ij} + \frac{(\xi^l_H - Z\xi^l_h)}{f(Z)}\frac{\sqrt{2}}{g}\left(\frac{m_W}{m_{d_i}}\right)(\tilde{Y}^{l}_{n(Z)})_{ij}\right]h^0 \\
&+i\left[-Z\delta_{ij} + f(Z)\frac{\sqrt{2}}{g}\left(\frac{m_W}{m_{d_i}}\right)(\tilde{Y}^{l}_{n(Z)})_{ij}\right]\gamma^5 A^0\Bigg\} l_j\Bigg),
\end{aligned}
\tag{2.23}
$$

where $V_{\rm CKM}$ denotes the mixing matrices of the quark sector, the functions $f_(x)$ and $n(x)$ are given by:

$$
\begin{aligned}
f(x) &= \sqrt{1+x^2}, \\
n(x) &= \begin{cases} 2 & \text{if } x = \tan\beta, \\ 1 & \text{if } x = \cot\beta. \end{cases}
\end{aligned}
\tag{2.24}
$$

the parameters $X$, $Y$, $Z$ are given in Refs. [62, 13, 15, 14, 26, 17, 80] and the factors $\xi^f_\phi$ are presented in Ref. [17]. Following this notation, the parameters for the framework 2HDM-(I,II,X,Y)-like can be listed through Tab. 2.1.

Following the analysis in [43],it is possible to derive a better approximation for the product $V_q\, Y^q_n\, V^\dagger_q$, expressing the rotated matrix $\tilde{Y}^q_n$, in the form

$$
\left[\tilde{Y}^q_n\right]_{ij} = \frac{\sqrt{m^q_i m^q_j}}{v}\,\left[\tilde{\chi}^q_n\right]_{ij} = \frac{\sqrt{m^q_i m^q_j}}{v}\,\left[\chi^q_n\right]_{ij}\, e^{i\vartheta^q_{ij}},
\tag{2.25}
$$

where the $\chi$'s are unknown dimensionless parameters of the model. They are consequence of the election of a specific texture of the Yukawa matrices. Eq. (2.25) is a consequence of the diagonalization process of Yuwaka matrices, assuming the hierarchy among the fermion masses [43], namely, the Cheng-Sher ansatz is a particular case of this parametrization. In order to have an acceptable model, the $\chi$'s parameters can be generally $O(1)$, but the will not be greater. It has been calculated the $\chi^2$ fit of Yukawa matrices including the CKM matrix, and it was found that the off-diagonal parameters are $O(1)$ (e.g., $\chi^f_{23} \leq 10$), therefore it is not possible to ignore all of these [47]. Besides, in Ref. [24], it is studied the general 2HDMs considering renormalization group evolution of the Yukawa couplings and the cases when the $\mathcal{Z}_2$-symmetry is broken, called non-diagonal models (e.g., the models with a structure incorporating the Cheng-Sher ansatz). It is notable that the off-diagonal elements in the down-sector are actually those that become large whereas the ones in the up-sector $\chi^u(\mu) \leq 0.1$, assuming the conservative criterion $\chi^f \leq 0.1$, where $\mu$ is the renormalization scale. On the other hand, the FCNC processes at low energy are going to determine bounds for these parameters with high precision, an aspect which is studied in this work. In order to perform the phenomenological study, it is convenient to rewrite the Lagrangian given in

eq. (2.23) in terms of the coefficients $[\tilde{\chi}^q_n]_{ij}$, as follows:

$$\begin{aligned}
\mathcal{L}^{\bar{f}_i f_j \phi} &= -\frac{g}{2\sqrt{2}M_W}\Bigg[\sum_{l=1}^{3}\bar{u}_i\Bigg[(V_{\rm CKM})_{il}\left(X\, m_{d_l}\,\delta_{lj} - \frac{f(X)}{\sqrt{2}}\sqrt{m_{d_l}m_{d_j}}\,\tilde{\chi}^d_{lj}\right)(1+\gamma^5) \\
&+\left(Y\, m_{u_i}\,\delta_{il} - \frac{f(Y)}{\sqrt{2}}\sqrt{m_{u_i}m_{u_l}}\,\tilde{\chi}^u_{il}\right)(V_{\rm CKM})_{lj}(1-\gamma^5)\Bigg] d_j\, H^+ \qquad (2.26)\\
&+\bar{\nu}_i\left(Z\, m_{l_i}\,\delta_{ij} - \frac{f(Z)}{\sqrt{2}}\sqrt{m_{l_i}m_{d_j}}\,\tilde{\chi}^l_{ij}\right)(1+\gamma^5) l_j H^+ + h.c.\Bigg] \\
&-\frac{g}{2M_W}\Bigg[\bar{d}_i\Bigg(\left[m_{d_i}\xi^d_H\delta_{ij} - \frac{(\xi^d_h + X\xi^d_H)}{f(X)}\frac{\sqrt{m_{d_i}m_{d_j}}}{\sqrt{2}}\tilde{\chi}^d_{ij}\right]H^0 \\
&+\left[m_{d_i}\xi^d_h\delta_{ij} + \frac{(\xi^d_H - X\xi^d_h)}{f(X)}\frac{\sqrt{m_{d_i}m_{d_j}}}{\sqrt{2}}\tilde{\chi}^d_{ij}\right]h^0 \\
&+i\left[-m_{d_i}X\delta_{ij} + f(X)\frac{\sqrt{m_{d_i}m_{d_j}}}{\sqrt{2}}\tilde{\chi}^d_{ij}\right]\gamma^5 A^0\Bigg) d_j \\
&u_i\Bigg(\left[m_{u_i}\xi^u_H\delta_{ij} + \frac{(\xi^u_h - Y\xi^u_H)}{f(Y)}\frac{\sqrt{m_{u_i}m_{u_j}}}{\sqrt{2}}\tilde{\chi}^u_{ij}\right]H^0 \\
&+\left[m_{u_i}\xi^u_h\delta_{ij} - \frac{(\xi^u_H + Y\xi^u_h)}{f(Y)}\left(\frac{\sqrt{m_{u_i}m_{u_j}}}{\sqrt{2}}\right)\tilde{\chi}^u_{ij}\right]h^0 \\
&+i\left[-m_{u_i}Y\delta_{ij} + f(Y)\frac{\sqrt{m_{u_i}m_{u_j}}}{\sqrt{2}}\tilde{\chi}^u_{ij}\right]\gamma^5 A^0\Bigg) u_j \\
&+\bar{l}_i\Bigg(\left[m_{l_i}\xi^l_H\delta_{ij} - \frac{(\xi^l_h + Z\xi^l_H)}{f(Z)}\frac{\sqrt{m_{l_i}m_{l_j}}}{\sqrt{2}}\tilde{\chi}^l_{ij}\right]H^0 \\
&+\left[m_{l_i}\xi^l_h\delta_{ij} + \frac{(\xi^l_H - Z\xi^l_h)}{f(Z)}\frac{\sqrt{m_{l_i}m_{l_j}}}{\sqrt{2}}\tilde{\chi}^l_{ij}\right]h^0 \\
&+i\left[-m_{l_i}Z\delta_{ij} + f(Z)\frac{\sqrt{m_{l_i}m_{l_j}}}{\sqrt{2}}\tilde{\chi}^l_{ij}\right]\gamma^5 A^0\Bigg) l_j\Bigg], \qquad (2.27)
\end{aligned}$$

where $[\tilde{\chi}^u_1]_{ij} = \tilde{\chi}^u_{ij}$, $[\tilde{\chi}^d_2]_{ij} = \tilde{\chi}^d_{ij}$ and $[\tilde{\chi}^l_2]_{ij} = \tilde{\chi}^l_{ij}$ have been redefined. Then, from eq. (2.26), the couplings $\bar{f}_i f_j \phi^0$, $\bar{u}_i d_j H^+$ and $u_i \bar{d}_j H^-$ are given by:

$$\begin{aligned}
g_{h^0\bar{f}_i f_j} &= -\frac{ig}{2M_W}(m_{f_i}h^f_{ij}), \quad g_{H^0\bar{f}_i f_j} = -\frac{ig}{2M_W}(m_{f_i}H^f_{ij}), \quad g_{A^0\bar{f}_i f_j} = -\frac{ig}{2M_W}(m_{f_i}A^f_{ij}\gamma_5), \\
g_{H^+\bar{u}_i d_j} &= -\frac{ig}{2\sqrt{2}M_W}(S_{ij} + P_{ij}\gamma_5), \quad g_{H^-u_i\bar{d}_j} = -\frac{ig}{2\sqrt{2}M_W}(S_{ij} - P_{ij}\gamma_5). \qquad (2.28)
\end{aligned}$$

where $h^f_{ij}$, $H^f_{ij}$, $A^f_{ij}$, $S_{ij}$ and $P_{ij}$ are defined as:

$$\begin{aligned}
h^d_{ij} &= \xi^d_h\delta_{ij} + \frac{(\xi^d_H - X\xi^d_h)}{\sqrt{2}f(X)}\sqrt{\frac{m_{d_j}}{m_{d_i}}}\tilde{\chi}^d_{ij}, \quad h^l_{ij} = h^d_{ij}(d\to l,\ X\to Z), \\
H^d_{ij} &= \xi^d_H\delta_{ij} - \frac{(\xi^d_h + X\xi^d_H)}{\sqrt{2}f(X)}\sqrt{\frac{m_{d_j}}{m_{d_i}}}\tilde{\chi}^d_{ij}, \quad H^l_{ij} = H^d_{ij}(d\to l,\ X\to Z), \qquad (2.29)\\
A^d_{ij} &= -X\delta_{ij} + \frac{f(X)}{\sqrt{2}}\sqrt{\frac{m_{d_j}}{m_{d_i}}}\tilde{\chi}^d_{ij}, \quad A^l_{ij} = A^d_{ij}(d\to l,\ X\to Z), \\
h^u_{ij} &= \xi^u_h\delta_{ij} - \frac{(\xi^u_H + Y\xi^u_h)}{\sqrt{2}f(Y)}\sqrt{\frac{m_{u_j}}{m_{u_i}}}\tilde{\chi}^u_{ij}, \\
H^u_{ij} &= \xi^u_H\delta_{ij} + \frac{(\xi^u_h - Y\xi^u_H)}{\sqrt{2}f(Y)}\sqrt{\frac{m_{u_j}}{m_{u_i}}}\tilde{\chi}^u_{ij}, \\
A^u_{ij} &= -Y\delta_{ij} + \frac{f(Y)}{\sqrt{2}}\sqrt{\frac{m_{u_j}}{m_{u_i}}}\tilde{\chi}^u_{ij}, \\
S_{ij} &= m_{d_j}\,X_{ij} + m_{u_i}\,Y_{ij}, \quad P_{ij} = m_{d_j}\,X_{ij} - m_{u_i}\,Y_{ij}, \qquad (2.30)
\end{aligned}$$

| 2HDM-III | $X$ | $Y$ | $Z$ | $\xi_h^u$ | $\xi_h^d$ | $\xi_l^d$ | $\xi_H^u$ | $\xi_H^d$ | $\xi_H^l$ |
|---|---|---|---|---|---|---|---|---|---|
| 2HDM-I-like | $-\cot\beta$ | $\cot\beta$ | $-\cot\beta$ | $c_\alpha/s_\beta$ | $c_\alpha/s_\beta$ | $c_\alpha/s_\beta$ | $s_\alpha/s_\beta$ | $s_\alpha/s_\beta$ | $s_\alpha/s_\beta$ |
| 2HDM-II-like | $\tan\beta$ | $\cot\beta$ | $\tan\beta$ | $c_\alpha/s_\beta$ | $-s_\alpha/c_\beta$ | $-s_\alpha/c_\beta$ | $s_\alpha/s_\beta$ | $c_\alpha/c_\beta$ | $c_\alpha/c_\beta$ |
| 2HDM-X-like | $-\cot\beta$ | $\cot\beta$ | $\tan\beta$ | $c_\alpha/s_\beta$ | $c_\alpha/s_\beta$ | $-s_\alpha/c_\beta$ | $s_\alpha/s_\beta$ | $s_\alpha/s_\beta$ | $c_\alpha/c_\beta$ |
| 2HDM-Y-like | $\tan\beta$ | $\cot\beta$ | $-\cot\beta$ | $c_\alpha/s_\beta$ | $-s_\alpha/c_\beta$ | $c_\alpha/s_\beta$ | $s_\alpha/s_\beta$ | $c_\alpha/c_\beta$ | $s_\alpha/s_\beta$ |

Table 2.1: Parameters $X$, $Y$ and $Z$ defined in the Yukawa interactions of eq. (2.23) for four versions of the 2HDM-III with a four-zero texture, which come from eqs. (2.19)–(2.22). Here $s_\alpha = \sin\alpha$, $c_\alpha = \cos\alpha$, $s_\beta = \sin\beta$ and $c_\beta = \cos\beta$.

with

$$\begin{aligned} X_{ij} &= \sum_{l=1}^{3}(V_{\rm CKM})_{il}\left[X\,\frac{m_{d_l}}{m_{d_j}}\,\delta_{lj} - \frac{f(X)}{\sqrt{2}}\sqrt{\frac{m_{d_l}}{m_{d_j}}}\,\tilde{\chi}^d_{lj}\right], \\ Y_{ij} &= \sum_{l=1}^{3}\left[Y\,\delta_{il} - \frac{f(Y)}{\sqrt{2}}\sqrt{\frac{m_{u_l}}{m_{u_i}}}\,\tilde{\chi}^u_{il}\right](V_{\rm CKM})_{lj}. \end{aligned} \tag{2.31}$$

For the case of leptons $S^l_{ij} = P^l_{ij}$

$$\begin{aligned} S^l_{ij} &= m_{l_j}\,Z^l_{ij}, \\ Z^l_{ij} &= \left[Z\,\frac{m_{l_i}}{m_{l_j}}\,\delta_{ij} - \frac{f(Z)}{\sqrt{2}}\sqrt{\frac{m_{l_i}}{m_{l_j}}}\,\tilde{\chi}^l_{ij}\right]. \end{aligned} \tag{2.32}$$

Then, the couplings $l_i^-\nu_{l_j}H^+$ and $l_i^+\nu_{l_j}H^-$ are given by

$$g_{H^+l_i^-\nu_{l_j}} = -\frac{ig}{\sqrt{2}M_W}S^l_{ij}\left(\frac{1+\gamma_5}{2}\right), \quad g_{H^-l_i^+\nu_{l_j}} = -\frac{ig}{\sqrt{2}M_W}S^l_{ij}\left(\frac{1-\gamma_5}{2}\right). \tag{2.33}$$

In order to compare these couplings with previous works [62, 13, 15, 14, 26, 17], it is convenient to define the couplings $\bar{u}_i d_j H^+$ and $u_i\bar{d}_j H^-$ in terms of the matrix elements $X_{ij}$, $Y_{ij}$ and $Z_{ij}$. Following the definitions (2.29)–(2.32), the following compact expression for the interactions of Higgs bosons with the fermions is obtained:

$$\begin{aligned} \mathcal{L}^{\bar{f}_i f_j \phi} &= -\left\{\frac{\sqrt{2}}{v}\overline{u}_i\left(m_{d_j}X_{ij}P_R + m_{u_i}Y_{ij}P_L\right)d_j\,H^+ + \frac{\sqrt{2}m_{l_j}}{v}Z_{ij}\overline{\nu_L}l_R H^+ + H.c.\right\} \\ &\quad -\frac{1}{v}\left\{\bar{f}_i m_{f_i}h^f_{ij}f_j h^0 + \bar{f}_i m_{f_i}H^f_{ij}f_j H^0 - i\bar{f}_i m_{f_i}A^f_{ij}f_j\gamma_5 A^0\right\}. \end{aligned} \tag{2.34}$$

When the parameters are $\chi^f_{ij} = 0$: $X_{11} = X_{22} = X_{33} = X$ (similarly for $Y$ and $Z$), the Yukawa interactions given in Refs. [62, 13, 15, 14, 17] are recovered. To hold consistencies with the MHDM/A2HDM [62], it could be that this Lagrangian could represent a MHDM/A2HDM with additional flavour physics in the Yukawa matrices as well as the possibility of FCNCs at tree level. Returning to the Lagrangian given in eq. (2.34), when the parameters $\chi^f_{ij}$ are present, it is possible to see that $X_{11} \neq X_{22} \neq X_{33} \neq X$, and the criteria of flavour constraints on $X$ are not possible to be applied directly to $X_{ij}$ (the same for $Y$ and $Z$), but the analyses for low energy processes are similar. Finally, it should be pointed out that parameters $X$, $Y$, $Z$, $\xi^f_\phi$ and $\chi_{ij}$ are arbitrary complex numbers, opening the possibility of having new sources of CP violation with tree-level FCNCs.

In Ref. [78], the flavour constraints of the 2HDM-III with a six-zero texture were studied, finding interesting results that can be used. However, both their results and the results presented in this work should be compared so as to distinguish the two parametrizations. Firstly, the six-zero texture assumed in [78] has been disfavoured by current data on the CKM mixing angles [51, 83]. Hence, the focus in this work is onto the four-zero texture, which is still acceptable phenomenologically and of which it considers the non-diagonal terms of the Yukawa matrices. Secondly, in order to unify notations, the parameters $\lambda^F_{ij}$ of [78] with parameters of this work $X_{ij}$, $Y_{ij}$ and $Z_{ij}$ as

given in eqs. (2.31) and (2.32), as follows[2]:

$$\begin{aligned}\mathcal{L}^{\bar{f}_i f_j H^+} &= -\Big\{\overline{u}_i\left(\sum_l^3 (V_{\rm CKM})_{il}\rho^D_{lj}P_R - \sum_l^3 \rho^U_{il}(V_{\rm CKM})_{lj}P_L\right) d_j\, H^+ \\ &\quad +\rho^l_{ij}\overline{\nu_L} l_R H^+ + H.c.\Big\}, \qquad (2.35)\\ \rho^F_{ij} &= \frac{\sqrt{2m_{Fi}m_{Fj}}}{v}\lambda^F_{ij}, \qquad (2.36)\end{aligned}$$

where $\rho^F_{ij}$ was introduced following the Cheng-Sher ansatz, considering $\lambda^F_{ij}\sim O(1)$. By comparing this with eq. (2.34), after using eqs. (2.31) and (2.32), the following relations are obtained:

$$\begin{aligned}\lambda^D_{ij} &= \left[X\sqrt{\frac{m_{d_i}}{m_{d_j}}}\,\delta_{ij} - \frac{f(X)}{\sqrt{2}}\,\tilde{\chi}^d_{ij}\right],\\ \lambda^U_{ij} &= -\left[Y\sqrt{\frac{m_{u_i}}{m_{u_j}}}\,\delta_{ij} - \frac{f(X)}{\sqrt{2}}\,\tilde{\chi}^u_{ij}\right],\\ \lambda^l_{ij} &= \left[Z\sqrt{\frac{m_{l_i}}{m_{l_j}}}\,\delta_{ij} - \frac{f(X)}{\sqrt{2}}\,\tilde{\chi}^l_{ij}\right], \qquad (2.37)\end{aligned}$$

and

$$\begin{aligned}X_{ij} &= \sum_l (V_{CKM})_{il}\sqrt{\frac{m_{d_l}}{m_{d_j}}}\lambda^D_{lj},\\ Y_{ij} &= \sum_l \sqrt{\frac{m_{u_l}}{m_{u_i}}}\lambda^U_{il}(V_{CKM})_{lj}. \qquad (2.38)\end{aligned}$$

This model could represent an effective flavour theory, wherein the Higgs fields necessarily participates in the flavour structure and has the same features as those of renormalizable flavour models [50, 49, 52, 19]. In this type of scenarios, a horizontal flavour symmetry, being it continuous or discrete, is added to the SM gauge group symmetry in such a way as to reproduce the observed mass and mixing angle patterns by only using renormalizable terms in the Lagrangians. This requirement has two consequences: firstly, there must be more than one $SU(2)$ doublet scalar; secondly, at least some of them must transform non-trivially under the flavour symmetry [18, 27].

## 2.8 Flavour constraints on the 2HDM-III with a four-zero Yukawa texture

Summarizing the constraints obtained in [66], the next constraints for the present work are acquired:

- $\mu - e$ universality in $\tau$ decays: Through requiring $\mu - e$ universality, the $\tau$ lepton decays into $\mu\bar{\nu}_\mu\nu_\tau$ and $e\bar{\nu}_e\nu_\tau$ constraint the charged Higgs boson states couplings to leptons [77, 73]. Following the analysis in [70], the following constraint is obtained with a 95% confidence level:

$$\frac{|Z_{22}Z_{33}|}{m^2_{H^\pm}} < 0.16 GeV^{-1}. \qquad (2.39)$$

- Leptonic meson decays: The leptonic decay of a charged meson, $M\to l\nu_l$ is sensitive to the charged Higgs exchange due to the helicity suppresion of the SM amplitude. constraints obtained from the decay $B\to\tau\nu$ are:

$$\frac{Z_{33}X_{13}}{m^2_{H^\pm}V_{ub}} \in [-0.036, 0.008]\, GeV^2 \bigvee [0.064, 0.108]\, GeV^2, \qquad (2.40)$$

and from the decay $D\to\mu\nu$ are

$$\frac{Z_{22}Y_{21}}{m^2_{H^\pm}V_{cd}} \in [-0.037, 0.035]\, GeV^2 \bigvee [0.535, 0.609]\, GeV^2. \qquad (2.41)$$

[2]It is adopted the description of the Yukawa sector presented in Ref. [78].

- $BR(B \to X_s\gamma)$: Following the analysis of [70, 93] and using standard values [25, 26, 98] for the charged Higgs boson mass (80 $GeV \leq m_{H^\pm} \leq$)300 $GeV$,the next constraints can be established:

$$\left|\frac{Y_{33}Y_{32}^*}{V_{tb}V_{ts}}\right| < 0.25,\ -1.7 < Re\left|\frac{X_{33}Y_{32}^*}{V_{tb}V_{ts}}\right| < 0.7. \tag{2.42}$$

- $B^0 - \bar{B}^0$ mixing: For a light charged Higgs boson (80 $GeV \leq m_{H^\pm} \leq$)200 $GeV$, the next limit can be extracted:

$$\left|\frac{Y_{33}^*Y_{31}}{V_{tb}V_{td}}\right| \leq 0.25. \tag{2.43}$$

- $Z \to b\bar{b}$: From [70] the combined limit from leptonic $\tau$ decays and the global fit (semi-)leptonic decays can be used, which is given by

$$\frac{|Y_{33}Z_{33}|}{m_{H^\pm}^2} < 0.005,\ |X_{33}| < 50. \tag{2.44}$$

- However, this constraint is contained in the $B \to X_s\gamma$ ones, which are more restrictive.

These constraints were used to compute the allowed regions of the model, so the computation of the cross sections could be done for processes that could be studied in the LHeC and the LHC.

# Chapter 3

# The $H^{\pm}$ production at the LHeC.

The 2HDM-III was constrained by taking into account the flavour and Higgs physics constraints, as well as the theoretical of the model, such as, vacuum stability, unitarity, perturbativity and various EW Precision Observables (EWPOs). The parameter space of the 2HDM-III is compatible with the SM-like Higgs boson. In this section, the production of a light charged Higgs boson at the future Large Hadron electron Collider (LHeC) wil be studied, through the process $e^- p \to \nu_e H^- q$ considering both decay channels $H^- \to b\bar{c}$ and $H^- \to \tau\bar{\nu}_\tau$ in the final state.

In order to carry out the numerical analysis, CalcHEP 3.6.29 [23] was used as parton level event generator, interfaced to the CTEQ6L1 Parton Distribution Functions (PDFs) [81], then PYTHIA6 [91] for the parton shower, hadronisation and hadron decays and PGS [35] as detector emulator, by using LHC parameter card suitably modified for the LHeC.

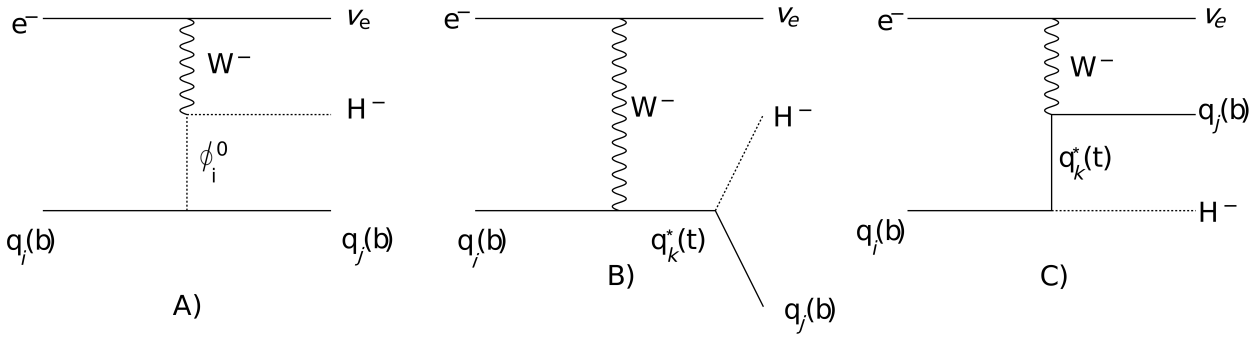


Figure 3.1: Feynman diagrams for the $e^-\ q \to \nu_e H^- q^{'}$ process. Here, $\phi_i^0 = h, H, A$, i.e., any of the neutral Hggs bosons of the BSM scenario considered here (see below).

## 3.1 Benchmark points and event rates

A series of programs were developed to compute the parameter space for the model. They rely on varying the $X$ and $Y$ variables, which depend on what scenario of the 2HDM-III has been chosen (I-like, II-like, X-like and Y-like). The method of computation begins with a C++ program, which does:

1. The four scenarios are configured, with certain parameters fixed.
2. The constraints given by (2.39-2.44) are taken into account. This part of the program takes into account the $\chi_{ij}^f$, $X_{ij}$, $Y_{ij}$, $Z_{ij}$, fermion masses, the CKM matrix elements, charged Higgs boson mass, meson masses, and the $X$, $Y$ and $Z$ parameters.
3. A loop to increase the values of $X$ and $Y$ is established. This defines how many and how fine the benchmark points will be generated.
4. The variables are printed into a specific bash file.

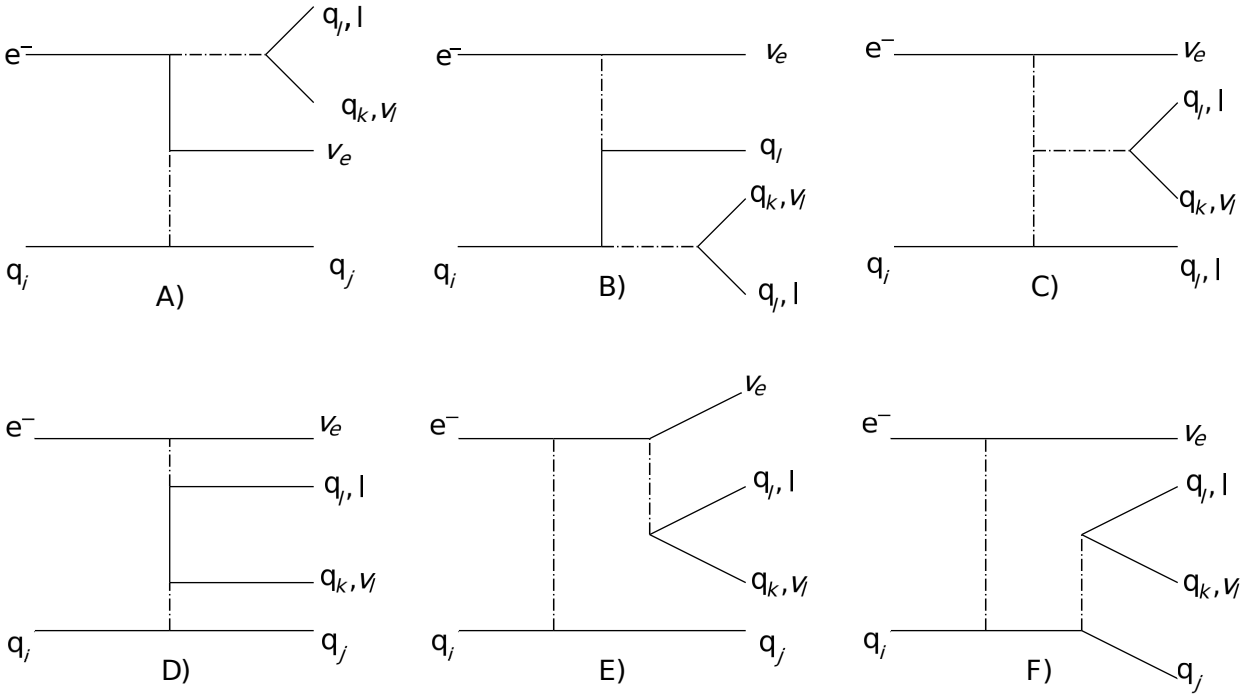


Figure 3.2: Feynman diagrams for the $\nu_e jjj$, $\nu_e bjj$ and $\nu_e bbj$ backgrounds (the change $q_l \leftrightarrow l$ and $q_k \leftrightarrow \nu_l$ represents the $\nu_e \nu_l lj$ and $\nu_e \nu_l lb$ backgrounds). Dash-dot lines represent boson fields: (pseudo)scalars and EW gauge bosons.

A set of bash files are generated if the program is run properly. Each of these generated files contain CalcHEP commands to set the program to compute under the conditions given by each one of them. The next step is to run each file, which can be many, in CalcHEP to obtain the branching ratios and the cross sections. This is done with the help of bash programs which will execute CalcHEP for each of the generated files and save the results given by it. The results obtained are for the cases of charged Higgs masses $h^{\pm} = 110GeV$, $130GeV$, $150GeV$, $170GeV$, a heavy Higgs mass $H = 150GeV$, and the pseudosacalar mass $A = 100GeV$.

The last step is to use a set of bash programs that will extract:

- Each simultaneous $X$ and $Y$ values.
- Each $BR(H^{\pm} \to cb)$ according to the $X$ and $Y$ values.
- Each $\sigma eq \to \nu_e H^{\pm} q'$ also according to the $X$ and $Y$ values.
- Combine all the results the results in a format to be implemented in Mathematica. This step multiplies the branching ratio, the cross section, and a luminosity of $100 fb^{-1}$.

With the last file, it was proceeded to use it to plot the event rates by using Mathematica. The results can be seen in figures (3.4-3.5).

With these plots it is possible to assume the benchmark points which might be able to have a signal in the experiments. It has to be taken into account that the results obtained so far are at the partonic level. In table(3.1) the values for $X$,$Y$ and $Z$ are shown along with the cross sections and branching ratios.

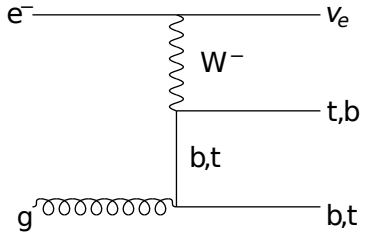


Figure 3.3: Feynman diagrams for the $\nu_e bt$ background.

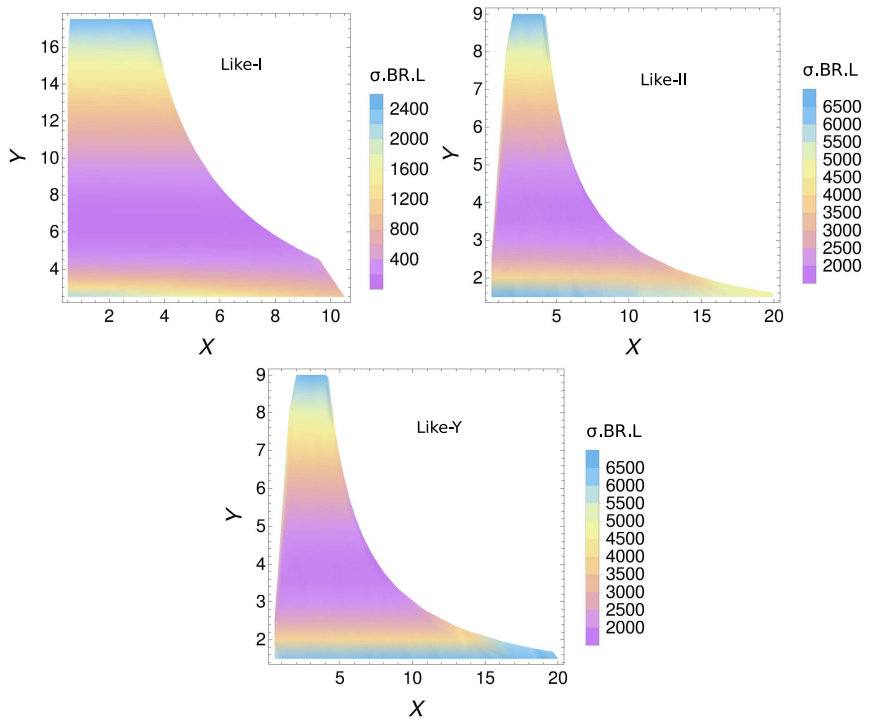


Figure 3.4: Event rates $\sigma.BR.L$ at the LHeC with $\sqrt{s_{ep}} \approx 1.3$ TeV, where $\sigma \equiv \sigma(ep \to \nu_e H^- q)$ with $q = q_l$ or $b$ is the production cross section, $L = 100$ fb$^{-1}$ is the integrated luminosity and BR is the decay fraction for the channel $H^- \to b\bar{c}$, for the following 2HDM-III scenarios: like-I (left), like-II (centre) and like-Y (right).

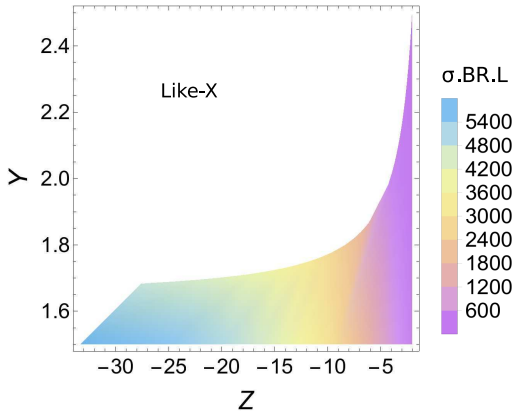


Figure 3.5: Event rates $\sigma.BR.L$ at the LHeC with $\sqrt{s_{ep}} \approx 1.3$ TeV, where $\sigma \equiv \sigma(ep \to \nu_e H^- q)$ with $q = q_l$ or $b$ is the production cross section, $L = 100$ fb$^{-1}$ is the integrated luminosity and BR is the decay fraction for the channel $H^- \to \tau\bar{\nu}_\tau$, for the following 2HDM-III scenario: like-X.

## 3.2 Simulation

An issue that appeared in the simulation was that the Pythia6 cards had to be adjusted to be able to compute electron-proton collisions in our case. This issue can be solved by adding into the card the command: MSTP(11) = 0. The MSTP(11) is the switch for the use of electron parton distribution in $e^+e^-$ and $ep$ interactions. By default the value is 1, which means that the electron carries only a fraction of beam energy in agreement with next-to-leading electron parton-distribution function, thereby including the effects of initial-state bremsstrahlung. By switching it to 0 the electron carries the whole beam energy, which is needed for this case.

Table 3.1: Parameter selection for benchmark points in the 2HDM-III: Here are present benchmark points for each incarnation of the 2HDM-III like-$I$, $II$, $Y$ and $X$. The first three scenarios have the variables selected so the $BR(H^{\pm} \to cb)$ is the main one. The last one has different values for the variables to increase the $BR(H^{\pm} \to \tau\nu_{\tau})$, so it is the main one.

| 2HDM-III like | parameters | | | $\sigma(ep \to \nu_e H^{\pm} q)[pb]$ | | | | $BR(H^{\pm} \to cb)$ | $BR(H^{\pm} \to \tau\nu_{\tau})$ |
|---|---|---|---|---|---|---|---|---|---|
| | x | y | z | $m_{H^{\pm}} = 110\ GeV$ | $130\ GeV$ | $150\ GeV$ | $170\ GeV$ | $m_{H^{\pm}} = 110\ GeV$ | $m_{H^{\pm}} = 110\ GeV$ |
| I | 0.5 | 17.5 | 0.5 | $2.56 \times 10^{-2}$ | $1.30 \times 10^{-2}$ | $3.47 \times 10^{-3}$ | $1.35 \times 10^{-4}$ | $9.57 \times 10^{-1}$ | $2.5 \times 10^{-4}$ |
| II | 2 | 1.5 | 2 | $2.18 \times 10^{-2}$ | $1.13 \times 10^{-2}$ | $2.95 \times 10^{-3}$ | $5.89 \times 10^{-5}$ | $9.9 \times 10^{-1}$ | $2.22 \times 10^{-4}$ |
| Y | 13 | 1.5 | -1/13 | $6.41 \times 10^{-2}$ | $3.27 \times 10^{-2}$ | $8.47 \times 10^{-3}$ | $2.2 \times 10^{-4}$ | $9.91 \times 10^{-1}$ | $6.12 \times 10^{-3}$ |
| X | 0.03 | 1.5 | -33.33 | $6.49 \times 10^{-2}$ | $3.39 \times 10^{-2}$ | $8.83 \times 10^{-3}$ | $2.34 \times 10^{-4}$ | $9.28 \times 10^{-2}$ | $9.04 \times 10^{-1}$ |

As intimated, in the framework of the 2HDM-III considered here, there are two main $H^{\pm}$ decay channels, which are $H^- \to b\bar{c}$ (the leading one for the incarnations like-I, -II and -Y) and $H^- \to \tau\bar{\nu}_{\tau}$ (the leading one for the incarnation like-X). Some BPs, maximising the signal rates in the four 2HDM-III incarnations defined in terms of the parameters $\chi_{ij}^{f}$ and $X, Y$ and $Z$ introduced previously, are given in Tab. 3.1, wherein the relevant $BR$s of the $H^{\pm}$ state are given alongside the cross sections of the associated production process $ep \to \nu_e H^- q$, where $q = q_l$ or $b$. (However, it was eventually verified that only the case $q = b$ is phenomenologically relevant, so that, henceforth, it was neglected discussing the case $q = q_l$ explicitly, though it is included in the simulations.)

The signatures that will be considered are as follows.

- On the one hand, in connection with the 2HDM-III like-I, -II and -Y, wherein the most relevant decay process is $H^- \to b\bar{c}$, the final state is $3j + \not{E}_T$ (where $j$ is a generic jet and $\not{E}_T$ refers to missing transverse energy), with one $b$-tagged and one light jet (associated to the charged Higgs boson reconstruction) accompanied by a remaining jet which can be $b$-tagged or not.
- On the other hand, in connection with the 2HDM-III like-X, wherein the most relevant decays process is $H^- \to \tau\bar{\nu}_{\tau}$, the final state is $j + l + \not{E}_T$, where $l = e, \mu$ (from a leptonic $\tau$ decay) and the jet is $b$-tagged.

The detector parameters simulated were as follows: a calorimeter coverage of $|\eta| < 5.0$ was considered, with segmentatiton $\Delta\eta \times \Delta\phi = 0.0359 \times 0314$ (the number of division in $\eta$ and $\phi$ are 320 and 200, respectively). Moreover, using Gaussian energy resolution, with

$$\frac{\Delta E}{E} = \frac{a}{\sqrt{E}} \oplus b, \tag{3.1}$$

where $a = 0.003$ and $b = 0.085$ for Electro-Magnetic (EM) calorimeter resolution or $b = 0.32$ for hadronic calorimeter resolution. The algorithm to perform jet finding was a"cone" with jet radius $\Delta R = 0.5$. The calorimeter trigger cluster finding a seed(shoulder) threshold was 5 GeV(1 GeV). It was taken $E_T(j) > 10$ GeV for a jet to be considered so, in addition to the isolation criterion $\Delta R(j; l) > 0.5$. Finally, the kinematic behaviour of the final state particles was mapped using MadAnalysis5 [34].

## 3.3 The process $e^-q \to \nu_e H^- b$ with $H^- \to b\bar{c}$ for the 2HDM-III like-I, -II and -Y

In this section the final state with one $b$-tagged jet and one light jet (associated with the secondary decay $H^- \to b\bar{c}$) alongside a generic (i.e., light or $b$-tagged) forward jet (associated with the primary collision) plus missing transverse energy will be discussed. For this case, the following cuts are applied[1].

1. First, events with exactly three jets in the final state are selected. Then, events without a $b$-tagged jet are rejected. Hence, at this point, events like $3j + \not{E}_T$ with at least one $b$-tagged jet are kept (Fig. 3.6). For these selections, the signal generally has an efficiency of 12% while the most efficient background $\nu_e bbj$ has a 10% response. The remaining backgrounds have efficiencies of 5%, 8% and 1% for $\nu_e bt$, $\nu_e bjj$ and $\nu_e jjj$, respectively.

[1]For illustration, it is assumed that the 2HDM-III like-Y scenario in the description, though the signal kinematics is essentially independent of the theoretical setup, as it primarily depends on the $m_{H^{\pm}}$ value.

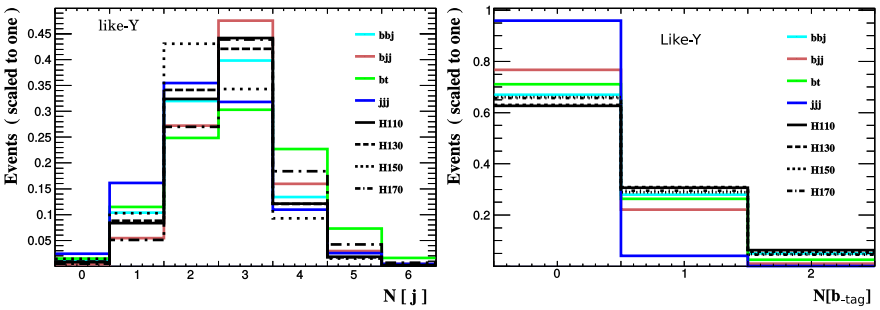


Figure 3.6: Distributions for the process $e^-q \to \nu_e H^- b$ followed by $H^- \to b\bar{c}$: in the left panel the multiplicity of all jets is shown while in the right panel the multiplicity of the $b$-tagged ones is presented. The like-Y case is illustrated. The normalisation is to the unity.

2. The second set of cuts is focused on selecting two jets (one $b$-tagged, labelled as $b_{\rm tag}$, and one not, labelled as $j_{\rm c}$) which are central in the detector. First, $P_T(b_{\rm tag}) > 30(40)$ GeV and $P_T(j_{\rm c}) > 20(30)$ GeV for $m_{H^\pm} = 110, 130(150, 170)$ GeV (here, $P_T$ is the transverse momentum) was demanded. Then, a cut on the pseudorapidity $|\eta(b_{\rm tag}, j_{\rm c})| < 2.5$ of both these jets and is imposed, finally, events in which $1.8(2) < \Delta R(j_{\rm c}; b_{\rm tag}) < 3.4(3.4)$ in correspondence of $m_{H^\pm} = 110, 130(150, 170)$ GeV (where $\Delta R$ is the standard cone separation) are selected. Upon enforcing these cuts, the signal has a cumulative efficiency of 7.3%. The most efficient background $\nu_e bjj$ has a rate of 6% while the others show efficiencies of 3.3%, 3.7% and 0.3% (for $\nu_e bt$, $\nu_e bbj$ and $\nu_e jjj$, respectively). This information is easily drawn from Fig. 3.7.

3. The next cut is related to the selection of a forward third generic jet (it can be either a light jet or a $b$-tagged one). The selection for such a third jet is $|\eta| > 0.6$ (with a transverse momentum above 20 GeV). With this cut, the signal shows an efficiency of 5.4% while 4.2% is the rate for the most efficient background ($\nu_e bjj$). The rest of the backgrounds show efficiencies below 2% for $\nu_e bbj$ and $\nu_e bt$ or 0.3% for $\nu_e jjj$.

4. The selection of the jet pair representing a $H^\pm$ candidate is made by considering only events for which the invariant mass of the two central jets is in the vicinity of the (trial) mass of the charged Higgs boson. However, it must be considered that, at the detector level, the signal may see a mass shift due to the finite efficiency in selecting the wanted jet dynamics. Therefore, in the histograms of Fig. 3.8, the invariant mass in the case of this signal is studied for, e.g., $m_{H^\pm} = 110$ (left) and 130 (right) GeV. These data is compared against the corresponding spectra from the backgrounds. From this plot, it can be seen a shift of the signal peaks towards lower invariant masses, so that it can be implemented the following selection criterium: $m_{H^\pm} - 20$ GeV $< M(b_{\rm tag}, j_{\rm c}) < m_{H^\pm}$. Furthermore, the invariant mass formed by the light central jet and the generic forward jet (not shown here) has a structure in most of the backgrounds, dictated by the presence of a hadronic $W^\pm$ boson decay. Because the signal does not have this feature, it is further imposed that $M(j_{\rm c}, j_{\rm f}) > 80$ GeV or $M(j_{\rm c}, j_{\rm f}) < 60$ GeV (where $j_{\rm f}$ labels the forward jet). This combination of mass cuts is highly selective, giving an overall efficiency of 2.4% for the signal and (at most) 0.6% for the backgrounds.

The final results, following the application of Cuts I–IV, are found in Tab. 3.2, for the 2HDM-III like-I, -II and -Y incarnations. Statistically, significances of the signal $\mathcal{S}$ over the cumulative background $\mathcal{B}$ are very good at low $H^\pm$ masses already for 100 fb$^{-1}$ of luminosity. As the latter increases, larger masses can be afforded through evidence or discovery, particularly so in the like-Y scenario. However, a ultimate mass reach is probably 130 GeV in all cases.

## 3.4 The process $e^-q \to \nu_e H^- b$ with $H^- \to \tau\bar{\nu}_\tau$ in the 2HDM-III like-X

Focusing on the channel $H^- \to \tau\bar{\nu}_\tau$, the leptonic $\tau$ decays ($\tau \to l\bar{\nu}_l\nu_\tau$, with $l = e, \mu$) and $b$-tagging the prompt (i.e., coming from the primary collision) jet in the final state have to be seen. The cuts to extract the signal are presented below.

1. This first set of cuts is focused on selecting events with one $b$-tagged jet and one lepton, by imposing $|\eta(b_{\rm tag}, l)| < 2.5$, $P_T(b_{\rm tag}, l) > 20$ GeV and the isolation condition $\Delta R(b_{\rm tag}; l) > 0.5$ (Fig. 3.9 for the histrograms of the lepton and jet multiplicities). Following this, the signal has an efficiency of 14% whereas

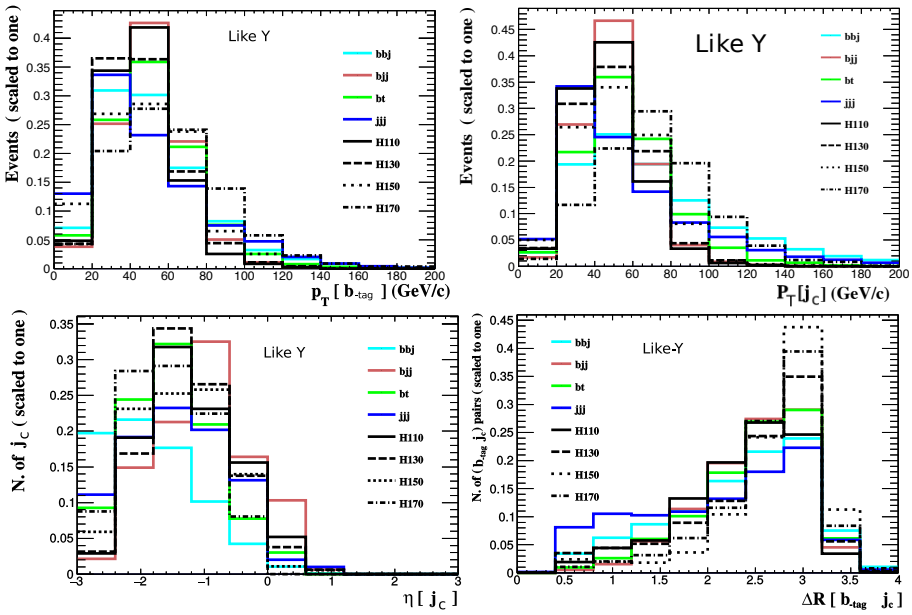


Figure 3.7: Distributions for the process $e^-q \to \nu_e H^- b$ followed by $H^- \to b\bar{c}$: in the top-left panel the transverse momentum of the central $b$-tagged jet is shown, in the top-right panel the transverse momentum of the central light jet, in the bottom-left panel the pseudorapidity of the central light jet while in the bottom-right panel the separation between the two central jets. The like-Y case is illustrated. The plot is normalised to the unity.

the backgrounds $\nu_e\nu_l lj$ and $\nu_e\nu_l lb$ have rates of 23% and 18%, respectively. The remaining noise shows an efficiency below 5%.

2. The next set of cuts enables to select a stiffer lepton and impose conditions on the missing transverse energy which are adapted to the trial $H^{\pm}$ mass. Events with $P_T(l) > 25(40)$ GeV and $\not{E}_T > 30(40)$ GeV for $m_{H^{\pm}} = 110,\ 130(150, 170)$ GeV are selected. The signal presents an efficiency of 70% while 80% is the rate for $\nu_e\nu_l lj$, $\nu_e\nu_l lb$ and $\nu_e tb$. The remaining backgrounds show efficiencies of 60% or below (Fig. 3.10).
3. Then, based on the left frame of Fig. 3.11, $|\eta(b_{\rm tag})| > 0.5$ is required. Furthermore, upon defining the total hadronic transverse energy $H_T = \sum_{\rm hadronic} |P_T|$ in the final state, based on the right frame of Fig. 3.11, select $H_T < 60$ GeV is selected. For the signal, these cuts are little discriminatory and show an efficiency of 75%. However, for all backgrounds, the efficiency is in general below 50%.
4. Finally, the last selection is done by exploiting the transverse mass $M_T(l)^2 = 2p_T(l)\not{E}_T(1 - \cos\phi)$, where $\phi$ is the relative azimuthal angle between $p_T(l)$ and $\not{E}_T$, a quantity which allows one to label the candidate events reconstructing the charged Higgs boson mass. However, the existence of one additional neutrino in the final state ($\nu_e$) emerging from the primary hard collision, alongside the two stemming from the $\tau$ decay

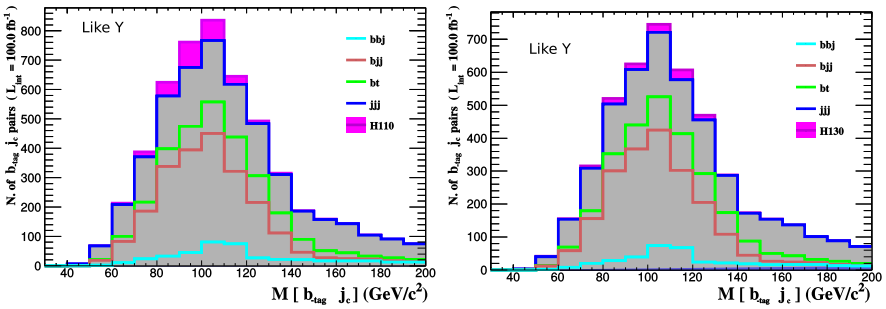


Figure 3.8: Distributions for the process $e^-q \to \nu_e H^- b$ followed by $H^- \to b\bar{c}$ in the invariant mass of the two central jets for $m_{H^{\pm}} = 110$ GeV (left) and $m_{H^{\pm}} = 130$ GeV (right). The like-Y case is illustrated. The normalisation is to the total event rate for $L = 100$ fb$^{-1}$.

| Signal | Scenario | Events (raw) | Cut I | Cut II | Cut III | Cut IV | $(\mathcal{S}/\sqrt{\mathcal{B}})_{100\,\mathrm{fb}^{-1}(1000\,\mathrm{fb}^{-1})[3000\,\mathrm{fb}^{-1}]}$ |
|---|---|---|---|---|---|---|---|
| $\nu_e H^{\pm} b$ | I-110 | 2562 | 298 | 182 | 134 | 54 | 1.43 (4.52) [7.82] |
| | I-130 | 1300 | 139 | 82 | 64 | 19 | 0.58 (1.82) [3.16] |
| | I-150 | 347 | 29 | 13 | 11 | 3 | 0.16 (0.5) [0.86] |
| | I-170 | 13 | 1.29 | 0.62 | 0.51 | 0.14 | 0.01 (0.03) [0.05] |
| $\nu_e H^{\pm} b$ | II-110 | 2183 | 245 | 151 | 122 | 53 | 1.4 (4.43) [7.68] |
| | II-130 | 1128 | 128 | 84 | 71 | 22 | 0.7 (2.21) [3.82] |
| | II-150 | 294 | 28 | 14 | 13 | 4 | 0.2 (0.65) [1.13] |
| | II-170 | 6 | 0.6 | 0.33 | 0.3 | 0.08 | 0.005 (0.017) [0.029] |
| $\nu_e H^{\pm} b$ | Y-110 | 6417 | 468 | 567 | 347 | 156 | 4.18 (12.99) [22.5] |
| | Y-130 | 3268 | 366 | 204 | 156 | 46 | 1.43 (4.53) [7.84] |
| | Y-150 | 847 | 68 | 29 | 23 | 6 | 0.33 (1.06) [1.83] |
| | Y-170 | 22 | 2.3 | 1.12 | 0.89 | 0.25 | 0.017 (0.05) [0.09] |
| $\nu_e bbj$ | | 20169 | 2011 | 748 | 569 | 125 | |
| $\nu_e bjj$ | | 117560 | 10278 | 7211 | 5011 | 718 | $\mathcal{B} = 1441$ |
| $\nu_e bt$ | | 41885 | 2278 | 1418 | 1130 | 188 | $\sqrt{\mathcal{B}} = 37.9$ |
| $\nu_e jjj$ | | 867000 | 9238 | 3221 | 2593 | 409 | |

Table 3.2: Significances obtained after the sequential cuts described in the text for the signal process $e^- q \to \nu_e H^- b$ followed by $H^- \to b\bar{c}$ for four BPs in the 2HDM-III like-I, -II and -Y. The simulation is done at detector level.

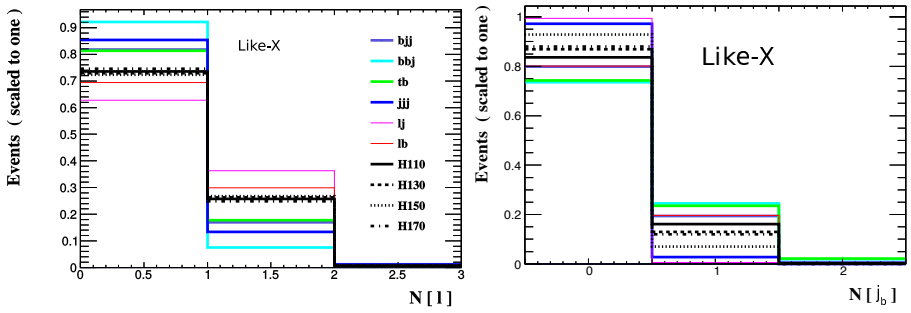


Figure 3.9: Distributions for the process $e^- q \to \nu_e H^- b$ followed by $H^- \to \tau\bar{\nu_\tau}$: in the left(right) panel the number of leptons($b$-jets) per event is presented. The like-X case is illustrated. The normalisation is to the unity.

($\nu_\tau$ and $\nu_l$), generates a widening of the transverse mass distribution of the signal. Therefore, the following selection is made: $m_{H^\pm} - 50$ GeV $< M_T(l) < m_{H^\pm} + 10$ GeV (Fig. 3.12). For this cut, the signal has a cumulative efficiency of 1%, quite comparable to the efficiency of $\nu lb$, which is 0.9%. The rest of the backgrounds are instead below 0.2%

The effectiveness of this selection strategy is confirmed by the final results in Tab. IV, wherein the signal and background rates are presented along with the corresponding significances after Cuts I–IV for the usual values of luminosity. Again, also in the like-X case, good sensitivity exists up to $H^{\pm}$ masses of 130 GeV.

## 3.5 Results

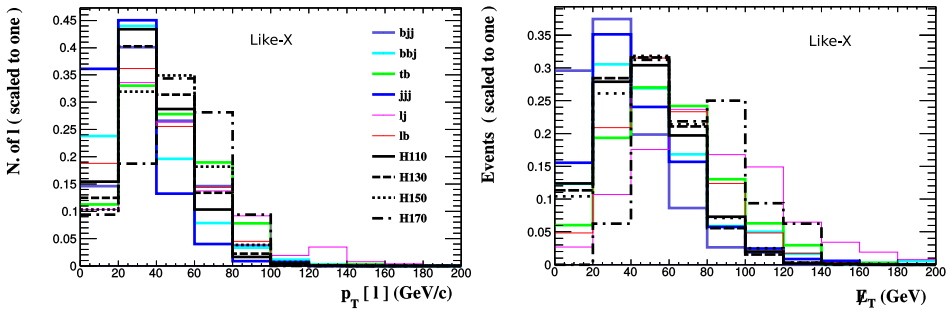


Figure 3.10: Distributions for the process $e^- q \to \nu_e H^- b$ followed by $H^- \to \tau \bar{\nu}_\tau$: in the left panel the transverse momentum of the lepton is presented, while in the right panel the total missing transverse energy is presented. The like-X case is illustrated. The normalisation is to the unity.

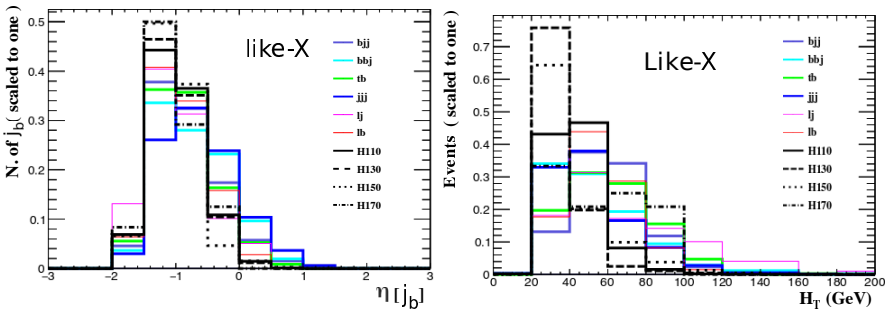


Figure 3.11: Distributions for the process $e^- q \to \nu_e H^- b$ followed by $H^- \to \tau \bar{\nu}_\tau$: in the left panel the pseudorapidity of the $b$ jet is presented, while in the right panel the total hadronic transverse energy. The like-X case is illustrated. The normalisation is to the unity.

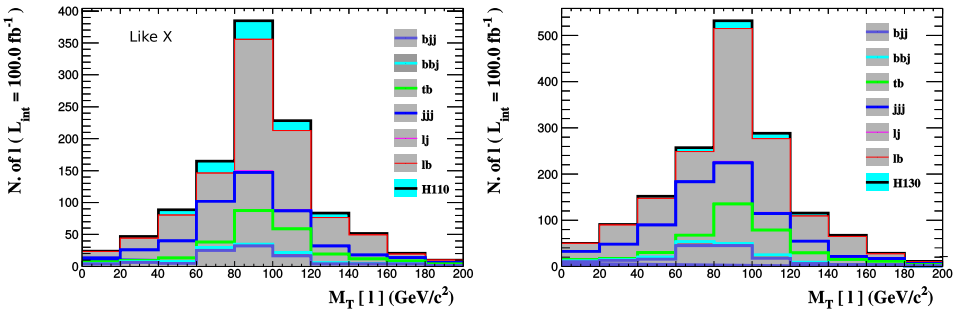


Figure 3.12: Distributions for the process $e^- q \to \nu_e H^- b$ followed by $H^- \to \tau \bar{\nu}_\tau$ in the transverse mass of the final state for $m_{H^\pm} = 110$ GeV (left) and $m_{H^\pm} = 130$ GeV (right). The like-X case is illustrated. The normalisation is to the total event rate for $L = 100$ fb$^{-1}$.

| Signal | Scenario | Events (raw) | Cut I | Cut II | Cut III | Cut IV | $(\mathcal{S}/\sqrt{\mathcal{B}})_{100\ \text{fb}^{-1}(1000\ \text{fb}^{-1})[3000\ \text{fb}^{-1}]}$ |
|---|---|---|---|---|---|---|---|
| $\nu_e H^- q$ | X-110 | 6480 | 178 | 124 | 94 | 67 | 2.41 (7.61) [13.19] |
| | X-130 | 3390 | 75 | 54 | 52 | 35 | 1.13 (3.58) [6.2] |
| | X-150 | 880 | 6 | 3 | 2 | 2 | 0.09 (0.29) [0.5] |
| | X-170 | 20 | 0.4 | 0.3 | 0.2 | 0.09 | 0.01 (0.02) [0.04] |
| $\nu_e bbj$ | | 20170 | 85 | 56 | 23 | 13 | |
| $\nu_e bjj$ | | 117559 | 623 | 340 | 122 | 84 | |
| $\nu_e tb$ | | 48845 | 460 | 374 | 149 | 105 | $\mathcal{B} = 763$ |
| $\nu_e jjj$ | | 867000 | 981 | 596 | 267 | 162 | $\sqrt{\mathcal{B}} = 27.62$ |
| $\nu_e l\nu_l j$ | | 23700 | 29 | 26 | 8 | 5 | |
| $\nu_e l\nu_l b$ | | 40400 | 1500 | 1203 | 569 | 392 | |

Table 3.3: Significances obtained after the sequential cuts described in the text for the signal process $e^- q \to \nu_e H^- b$ followed by $H^- \to \tau\bar{\nu}_\tau$ for four benchmark points in the 2HDM-III like-X. The simulation is done at detector level.

# Chapter 4

# The $H^{\pm}$ production at the LHC through quark fusion process.

In this thesis work, the case of the $H^{\pm}$ production at the LHC is studied throught the quark-fusion $cb \to H^{\pm}$. The model makes the quark-fusion production of the charged Higgs to be stronger for the cases of the $cb$ fusions. In this case the focus on the $H^{\pm} \to \tau\nu_{\tau}$ decay is to achieve cleaner signals in the experiment.

This case has very small cross sections for the Type-I-like, Type-II-like and Y-like scenarios, therefore the Type-X-like scenario is explored. It was seen that it was needed to check small $X$ parameter values. This is because of the $Z$ parameter becoming much more important in this case.

## 4.1 Benchmark Points

By taking into account both flavour and Higgs physics as well as EW Precision Observables (EWPOs) (e.g., the oblique parameters) plus theoretical bounds such as vacuum stability, unitarity as well as perturbativity. This work focuses to the parameter space region where $m_h = 125$ GeV (hence, $h$ is the SM-like Higgs boson), with $m_A = 100$ GeV, 180 GeV $< m_H <$ 260 GeV and 100 GeV$< m_{H^{\pm}} <$ 170 GeV, further assuming $\cos(\beta - \alpha) = 0.1$, 0.5. The oblique parameter $U = 0$ is fixed, since that $U$ is suppressed by a factor of order the new physics scale $\Lambda^2$ compared to the parameters $S$ and $T$ [92], where: $S = 0.02 \pm 0.07$ and $T = 0.06 \pm 0.06$. In general, the parameter space of the 2HDM-III with the four-zero-texture considered here is fully compatible with the SM-like Higgs boson discovery [5], as it has been implemented the same analysis of Refs. [47, 66], wherein the radiative decays $h \to \gamma\gamma$, $\gamma Z$ were studied and the impact of the charged Higgs bosons flowing in the corresponding loops was analysed in detail. That study is adapted here by taking into account the most recent experimental data from the LHC for these two decay modes [87, 88, 1, 2, 3]: upon applying these filters, the mass of the light charged Higgs boson is constrained in the range 110 GeV$< m_{H^{\pm}} <$ 170 GeV with $\cos(\beta - \alpha) = 0.1$, 0.5. However, fermiophobic couplings for a charged Higgs boson with mass in the range 79 GeV$< m_{H^{\pm}} <$ 100 GeV are allowed in the light of the given experimental constraints. Furthermore, recent experimental bounds from flavour physics are considered here, following the analysis of Refs. [47, 66, 36], where the parameter space of the model is bound by leptonic and semi-leptonic meson decays, being the inclusive decay $B \to X_s\gamma$, $B_0 - B_0$ and $K_0 - K_0$ mixing as well as $B_s \to \mu^+\mu^-$ transitions the strongest constraints available. One can further get a scenario where a rather light charged Higgs mass is feasible, because the Yukawa-texture effects enter directly in the amplitudes of the mentioned mesonic decays, thus enabling one to evade these bounds. Resuming the current limits on the masses of the various Higgs bosons from direct searches at previous and current colliders:

- LEP limits. A lower limit of 114 GeV was imposed for both Higgs bosons which are CP-even states, whether SM-like or not, albeit the lower mass region is ambiguous given a slight excess observed at LEP for an invariant mass around 98 GeV [21]. In the MSSM configuration, for large $\tan\beta$ and low mass for the CP-odd Higgs boson, being the lightest Higgs boson $h$ non-SM-like, the limits on the neutral masses are: $m_A > 93.4$ GeV and $m_h > 92.8$ GeV [85]. Furthermore, from the Higgs-strahlung process, the LEP collaborations have established as lower bound for the heavy neutral Higgs bosons mass of 112 GeV [71]. For the mass of the charged Higgs boson, the LEP collaborations have instead established a lower bound at 78.6 GeV [85].
- Tevatron limits. The CDF collaboration reported a local excess in the mass region 130 GeV $< m_h <$ 160 GeV [6] and D0 found a local fluctuation in the $H^{\pm}$ mass region from 110 GeV to 125 GeV [8]. These are

consistent with the later discovery of the 125 GeV state. For the case of a mass of the charged Higgs boson in the range 90 GeV to 160 GeV, the CDF and D0 experiments extracted a limit for the BR($t \to H^+ b$) of $\approx 20\%$ considering both cases BR($H^+ \to c\bar{s}$) = 1 and BR($H^+ \to \tau^+ \nu$) = 1 [9, 10, 7].

- LHC limits. The almost degenerate case for the masses of Higgs bosons in the range 110 GeV $< m_H <$ 150 GeV has been analysed by CMS and the experimental results can be applied in a generic way to a CP-odd state too [32]. The case of additional states with exactly the same mass of the discovered Higgs boson (when it is SM-like) is not discarded and some models could reproduce it, as it would be case for the 2HDM-I [16]. In contrast, a fermiophobic Higgs boson with mass in the range 110 GeV to 188 GeV has been excluded by CMS [31]. Concerning CP-odd states, lately, the CMS collaboration has reported a slight excess with a mass just above 97.6 GeV [33]. However, the ATLAS experiment has not observed a corresponding significant excess [92]. Besides, recently, the CMS collaboration has excluded small values of $\tan\beta$ in the framework of any 2HDM in the range 225 GeV $< m_A <$ 1000 GeV [89]. For the analysis of a charged Higgs boson, CMS has set BR($t \to H^+ b$) = $2 - 3\%$ as upper limit for the case BR($H^+ \to \tau^+ \nu$) = 1 in the range of masses varying from 80 GeV to 160 GeV [92]. Otherwise, assuming BR($H^+ \to c\bar{s}$) = 1, ATLAS and CMS set BR($t \to H^+ b$) $\approx 20\%$ for the mass range 90 GeV to 160 GeV [92]. Finally, quite recently, CMS set a limit of BR($t \to H^+ b$) = $0.5 - 0.8\%$ for the case BR($H^+ \to c\bar{b}$) = 1 in the mass range 90 GeV to 150 GeV [86].

Considering all experimental bounds and theoretical constraints, it is proceeded to choose several scenarios. Specifically, four scenarios are considered, wherein relevant Benchmarks Points (BPs) are defined according to the standard Yukawa prescriptions: Type I (where one Higgs doublet couples to all fermions); Type II (where one Higgs doublet couples to the up-type quarks and the other to the down-type quarks); Type X (also called IV or "Lepton-specific", where the quark couplings are Type I and the lepton ones are Type II); Type Y (also called III or "Flipped" model, where the quark couplings are Type II and the lepton ones are Type I).

For a light charged Higgs boson, in the 2HDM-III, the most important decay channels are $H^- \to s\bar{c}$ and $b\bar{c}$, when $Y \gg X, Z$ (like-I scenario), $X$, $Z \gg Y$ (like-II scenario) or $X \gg Y$, $Z$ (like-Y scenario), in which cases the mode $H^- \to b\bar{c}$ receives a substantial enhancement, coming from the four-zero-texture implemented in the Yukawa matrices, so as to obtain even a BR($H^- \to b\bar{c}$) $\approx 0.95$, so that the focus is on this decay, also owing to the fact that it can be $b$-tagged, thus reducing in turn the level of background. However, for the case $Z \gg X, Y$ (like-X scenario), the decay channel $H^- \to \tau\bar{\nu}_\tau$ is maximised, reaching a $B$R of 90 % or so [66], so that this mode shall be studied, because the production $c\bar{b} + h.c. \to \tau\nu$ can reach considerable cross section. For the latter scenario $BR(H^{\pm} \to \tau\nu) \approx 0.9$ and $BR(H^{\pm} \to cb) \approx 0.1$, and considering the parameter scan performed in [37], the following BP are adopted, where production of a light charged Higgs boson trough $\sigma(c\bar{b} \to H^+ \to \tau\bar{\nu}_\tau)$ offer the most optimistic chances for detection:

- Scenario 2HDM-III like-X: $\cos(\beta - \alpha) = 0.5$, $\chi^u_{22} = 1$, $\chi^u_{23} = 0.1$, $\chi^u_{33} = 1.4$, $\chi^d_{22} = 1.8$, $\chi^d_{23} = 0.1$, $\chi^d_{33} = 1.2$, $\chi^\ell_{22} = -0.4$, $\chi^\ell_{23} = 0.1$, $\chi^\ell_{33} = 1$ with $Z \gg X$, $Y$.

For all these scenarios, it is assumed that $m_h = 125$ GeV and considered $m_A = 100$ GeV, $m_H = 150$ GeV.

## 4.2 Scenarios

The case of the $H^{\pm}$ production at the LHC is studied throught the quark-fusion $cb \to H^{\pm}$. The model makes the quark-fusion production of the charged Higgs to be stronger for the cases of the $cb$ fusions. In this case the focus on the $H^{\pm} \to \tau\nu_\tau$ decay is to achieve cleaner signals in the experiment.

This case has very small cross sections for the Type-I-like, Type-II-like and Y-like scenarios, therefore the Type-X-like scenario is explored. It was seen that it was needed to check small $X$ parameter values. This is because of the $Z$ parameter becoming much more important in this case. The benchmark points scan was done by using the parameter space permitted by experimental data and theoretical constraint, and by forcing CalcHEP to compute $pp \to H^{\pm} \to \tau\nu_\tau$. The constraints given in the Section (4.1) are taken again into account, and also includes constraints given by the CMS collaboration for the $BR(h \to b\bar{b})$, $BR(t \to H^{\pm} b)$ and the $\sigma(pp \to tbH^{\pm})$ [90]. After the benchmark points were computed and plotted, the best points were tested one last time to verify if they could pass the CMS constraints for the charged Higgs boson search. Having the allowed region, since the $X$ range was to small, it was decided to plot $Z - Y$ instead of $X - Y$. The event rates obtained showed that the number of events were still small enough to not be seen in the simulations. In Fig. 4.1 the event rates can be seen. So the $\chi^{33}_l$ parameter was varied with the intention of finding a better case. After seeing that $\chi^{33}_l = 0.5$ was big enough and passed all the constraints, it was determined to use that value.

For this scenario it is considered a mass range for the $H^{\pm}$ between $120GeV$ and $750GeV$. The best point is for the point $X = 0.04$, $Y = 1.6$, $Z = -20$, which has $\approx 2.276 \times 10^6$ events for $M_{H^{\pm}} = 120GeV$.

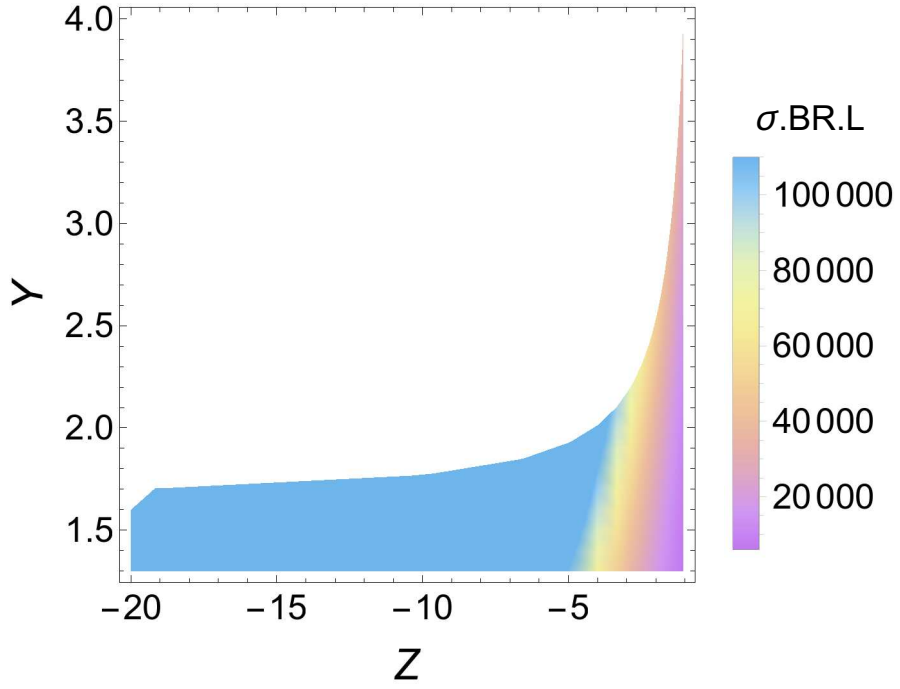


Figure 4.1: Benchmark points and event rates for the Scenario-X: $\chi^{\ell}_{33} = 0.5$, $\cos(\beta-\alpha) = 0.1$, $\chi^{u}_{22} = 1$, $\chi^{u}_{33} = 1.4$, $\chi^{d}_{22} = 1.8$, $\chi^{d}_{33} = 1.2$, $\chi^{u,d}_{23} = 0.1$, $\chi^{\ell}_{22} = -0.4$, $\chi^{\ell}_{23} = 0.1$, $m_A = 100$ GeV and $m_{H^{\pm}} = 120$ GeV. Due to Mathematica limitations, the event rates of the best points can not be shown.

## 4.3 Simulation

The Background for the quark-fusion process $q_1 q_2 \to H^{\pm} \to \tau\nu_{\tau}$ at the LHC was taken as $q_1 q_2 \to W^{\pm} \to l\nu_l$. As previously stated, the idea behind taking this process into account is to focus on the leptonic decays, so the signals may be cleaner than a decay involving quarks. Still, the noise generated by a proton-proton collision showed that the scenarios I-like, II-like and Y-like had not enough events to be seen in the experiment. Proceeding with the X-like case was the best option to study.

In the framework of the 2HDM-III considered here, there are two main $H^{\pm}$ decay channels, which is $H^{\pm} \to \tau\nu$ (the leading one for the incarnation like-X). Some BPs, maximising the signal rates in the four 2HDM-III incarnations defined in terms of the parameters $\chi^{f}_{ij}$ and $X, Y$ and $Z$ introduced previously, are given in Tab. 3.1, wherein the relevant $BR$s of the $H^{\pm}$ state are given alongside the cross sections of the associated production process $c\bar{b} + h.c. \to \tau\nu$. The signatures that will be considered are as follows.

- In connection with the 2HDM-III like-X, wherein the most relevant decays process is $H^{\pm} \to \tau\nu$, the final state is $l + \not{E}_T$, where $l = e, \mu$ (from a leptonic $\tau$ decay).

In order to carry out the numerical analysis, CalcHEP 3.6.29 [23] was used as Parton level event generator, interfaced to the CTEQ6L1 Parton Distribution Functions (PDFs) [81], then PYTHIA6 [91] for the Parton shower, hadronization and hadron decays and PGS [35] as detector emulator, by using an LHC parameter card. In particular, the detector parameters simulated were as follows: it is considered a calorimeter coverage $|\eta| < 5.0$, with segmentation $\Delta\eta \times \Delta\phi = 0.087 \times 0.10$ (the number of division in $\eta$ and $\phi$ are 320 and 200, respectively). Moreover, a Gaussian energy resolution was used, with

$$\frac{\Delta E}{E} = \frac{a}{\sqrt{E}} \oplus b, \tag{4.1}$$

where $a = 0.5$ and $b = 0.03$ both the Electro-Magnetic (EM) calorimeter resolution and for the hadronic calorimeter resolution, with $\oplus$ meaning addition in quadrature. Herein, the values of $a$ and $b$ are parameters established by the design of the LHC [11]. The algorithm to perform jet finding was a"cone" one with jet radius $\Delta R = 0.5$. The calorimeter trigger cluster finding a seed(shoulder) threshold was 5 GeV(1 GeV).

Again, the kinematic behaviour of the final state particles was mapped with MadAnalysis5 [34]. Six masses were selected for the charged Higgs boson: 120 GeV, 170 GeV, 200 GeV, 400 GeV, 500 GeV and 750 GeV. Also,

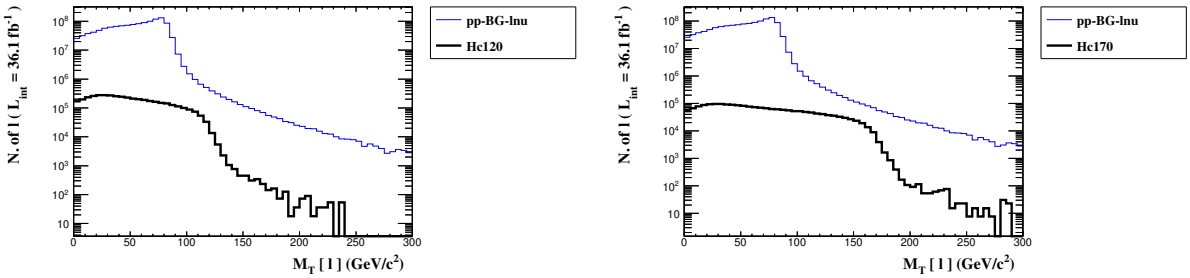


Figure 4.2: Transverse mass plots for signal and background, for selected $M_{H^{\pm}}$ choices of the former. No cuts are here applied.

it was demanded that jets would not be taken into account, to achieve the cleaner data. It was also demanded that at least one lepton was detected. In Fig. 4.2 the shape of the transverse mass plot with the basic setup cuts mentioned latter for both signal and background can be seen, Transverse mass stacked plot for the quark fusion process with setup cuts for $m_{H^{\pm}} = 120$, GeV (left) and $m_{H^{\pm}} = 170$, GeV (right). In order to fully define our selection, let us now investigate some relevant differential distributions that can be used to enhance the signal-to-background rate.

1. From the lepton and hadronic multiplicity plots, see Figs. 4.3 and 4.4, we require at least one lepton and impose no jets in our sample. (Here, we impose on both lepton and jets the acceptance region in transverse momentum and rapidity as already discussed: i.e., $p_T(l)$, $p_T(j) > 10$ GeV and $|\eta(l)|, |\eta(j)| < 3$ with $\Delta R(j,l) > 0.5$.) Further, by looking at Fig. 4.5 (wherein the jet veto is applied), it can be seen that the cut $p_T(l) \geq 45$ GeV on the leptonic transverse momentum can be profitably adopted for all charged Higgs mass boson masses.
2. The missing transverse energy plots, Fig. 4.6, suggest the use of the following cuts: for $M_{H^{\pm}} = 120$ GeV, 40 GeV $\leq \not{E}_T \leq 70$ GeV; for $M_{H^{\pm}} = 170$ GeV, 60 GeV $\leq \not{E}_T \leq 90$ GeV; for $M_{H^{\pm}} = 200$ GeV, 70 GeV $\leq \not{E}_T \leq 105$ GeV; for $M_{H^{\pm}} = 400$ GeV, 100 GeV $\leq \not{E}_T \leq 225$ GeV; for $M_{H^{\pm}} = 500$ GeV, 90 GeV $\leq \not{E}_T \leq 270$ GeV; for $M_{H^{\pm}} = 750$ GeV, 105 GeV $\leq \not{E}_T$.
3. The lepton pseudorapidity, Fig. 4.7, shows that an optimal cut can be defined for all charged Higgs boson masses as $|\eta(l)| \leq 1.2$.
4. The total energy, Fig. 4.8, shows that the following cuts can be efficient: for $M_{H^{\pm}} = 120$, 170 GeV, $E_T \geq 55$ GeV; for $M_{H^{\pm}} = 200$ GeV, $E_T \geq 60$ GeV; for $M_{H^{\pm}} = 400$ GeV, $E_T \geq 80$ GeV; for $M_{H^{\pm}} = 500$ GeV, $E_T \geq 75$ GeV; for $M_{H^{\pm}} = 750$ GeV, $E_T \geq 80$ GeV.
5. The transverse mass plots in Fig. 4.9 show that the last cuts to be defined can be as follows: for $M_{H^{\pm}} = 120$ GeV, 85 GeV $\leq M_T(l) \leq 125$ GeV; for $M_{H^{\pm}} = 170$ GeV, 90 GeV $\leq M_T(l) \leq 175$ GeV; for $M_{H^{\pm}} = 200$ GeV, 110 GeV $\leq M_T(l) \leq 205$ GeV; for $M_{H^{\pm}} = 400$ GeV, 170 GeV $\leq M_T(l) \leq 405$ GeV; for $M_{H^{\pm}} = 500$ GeV, 200 GeV $\leq M_T(l) \leq 505$ GeV; for $M_{H^{\pm}} = 750$ GeV, 320 GeV $\leq M_T(l) \leq 755$ GeV.

Following the above sequence of cuts, for which the signal and background responses can be found in table (4.3) the cuts of this analysis can be seen, we revisit in Fig. 4.10 the transverse mass distributions in the relevant peak regions. From these, the significances given in table4.3 can be extracted. In turn, from these, it can be concluded that the signal is strong enough to be detectable at the LHC over a very large mass range, covering both the light and heavy mass regime of the charged Higgs boson stemming from the 2HDM-III. In fact, by interpolating between the various charged Higgs boson masses used in the MC analysis, we can perform a continuous scan of the relevant 2HDM-III like-X parameter space surviving current theoretical and experimental limits and map the signal significances, obtained at $L = 36.1$ fb$^{-1}$ via the above search channel, in terms of the 2HDM-III input parameters to which the latter is sensitive, i.e., $\tan\beta$, $\chi^l_{33}$ (via $Y$) and $M_{H^{\pm}}$.

It can be concluded that, even if the model has to be very constrained, the signal is strong enough to be detectable at the LHC through the $H^{\pm} \to \tau\nu_{\tau}$ decay, as it can be seen in Fig. 4.10. These results are preliminary and further research will be done on this topic.

| $M_{H^{\pm}}$ | Cut 1: $p_T(l)$ | Cut 2: $\not{E}_T$ | Cut 3:$\lvert\eta(l)\rvert$ | Cut 4: $E_T$ | Cut 5: $M_T(l)$ |
|---|---|---|---|---|---|
| 120 GeV | $\geq 45$ GeV | $\geq 40$ GeV<br>$\leq 70$ GeV | $\leq 1.2$ GeV | $\geq 55$ GeV | $\geq 85$ GeV<br>$\leq 125$ GeV |
| Signal events | 294136 | 237167 | 175126 | 85480 | 82147 |
| Background events | 21413020 | 6568992 | 3054029 | 815194 | 815194 |
| 170 GeV | $\geq 45$ GeV | $\geq 60$ GeV<br>$\leq 90$ GeV | $\leq 1.2$ GeV | $\geq 55$ GeV | $\geq 90$ GeV<br>$\leq 175$ GeV |
| Signal events | 290051 | 138676 | 124849 | 114334 | 113758 |
| Background events | 21413020 | 1032667 | 520912 | 440061 | 423643 |
| 200 GeV | $\geq 45$ GeV | $\geq 70$ GeV<br>$\leq 105$ GeV | $\leq 1.2$ GeV | $\geq 60$ GeV | $\geq 110$ GeV<br>$\leq 205$ GeV |
| Signal events | 233230 | 94175 | 84981 | 80777 | 80453 |
| Background events | 21413020 | 493109 | 253526 | 230590 | 224650 |
| 400 GeV | $\geq 45$ GeV | $\geq 100$ GeV<br>$\leq 225$ GeV | $\leq 1.2$ GeV | $\geq 80$ GeV | $\geq 170$ GeV<br>$\leq 405$ GeV |
| Signal events | 42612 | 22833 | 20864 | 20714 | 20578 |
| Background events | 21413020 | 113851 | 60143 | 58740 | 56925 |
| 500 GeV | $\geq 45$ GeV | $\geq 90$ GeV<br>$\leq 270$ GeV | $\leq 1.2$ GeV | $\geq 75$ GeV | $\geq 200$ GeV<br>$\leq 505$ GeV |
| Signal events | 20674 | 14716 | 13292 | 13194 | 12021 |
| Background events | 21413020 | 183647 | 95536 | 92648 | 54368 |
| 750 GeV | $\geq 45$ GeV | $\geq 105$ GeV | $\geq 80$ GeV | $\geq 1$ GeV | $\geq 320$ GeV<br>$\leq 755$ GeV |
| Signal events | 4381 | 3351 | 3049 | 3042 | 2279 |
| Background events | 21413020 | 96691 | 51315 | 50243 | 8910 |

Table 4.1: Number of events after doing the multiplicity cuts of signal and background each cut described in the text, adopting the same sequence, $L = 36.1$ fb$^{-1}$.

| $H^{\pm}$ mass (GeV) | Signal | Background | $S/\sqrt{S+B}$ |
|---|---|---|---|
| 120 | 82147 | 621729 | 97.914 |
| 130 | 111026 | 591368 | 132.48 |
| 140 | 138553 | 676344 | 153.48 |
| 150 | 133205 | 571403 | 158.690 |
| 155 | 123148 | 502597 | 155.679 |
| 160 | 131734 | 533122 | 161.561 |
| 165 | 133767 | 540960 | 162.849 |
| 170 | 113758 | 423643 | 155.179 |
| 175 | 117716 | 429913 | 159.072 |
| 180 | 121355 | 446496 | 161.043 |
| 200 | 80453 | 224650 | 145.653 |
| 220 | 79475 | 225228 | 143.977 |
| 250 | 73119 | 241563 | 130.345 |
| 300 | 38855 | 84398 | 110.675 |
| 400 | 20578 | 56925 | 73.919 |
| 500 | 12021 | 54368 | 46.657 |
| 750 | 2279.4 | 8910.1 | 21.549 |
| 800 | 1643.8 | 8085.1 | 16.665 |
| 1000 | 637.5 | 4455.1 | 8.933 |

Table 4.2: Significances after the complete sequence of cuts described in the text with $L = 36.1$ fb$^{-1}$.

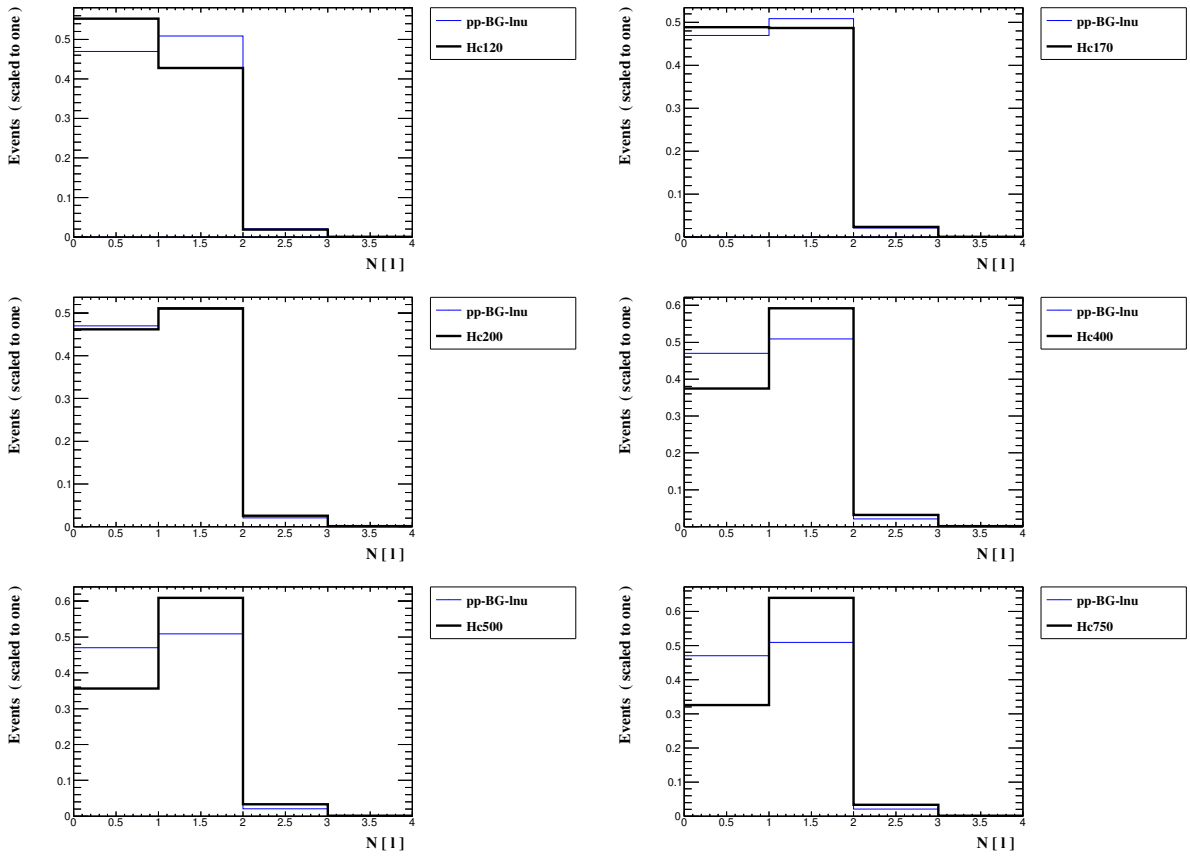


Figure 4.3: Lepton multiplicity plots for signal and background, for selected $M_{H^{\pm}}$ choices of the former, over the acceptance region for leptons and jets, in both transverse momentum as pseudorapidity.

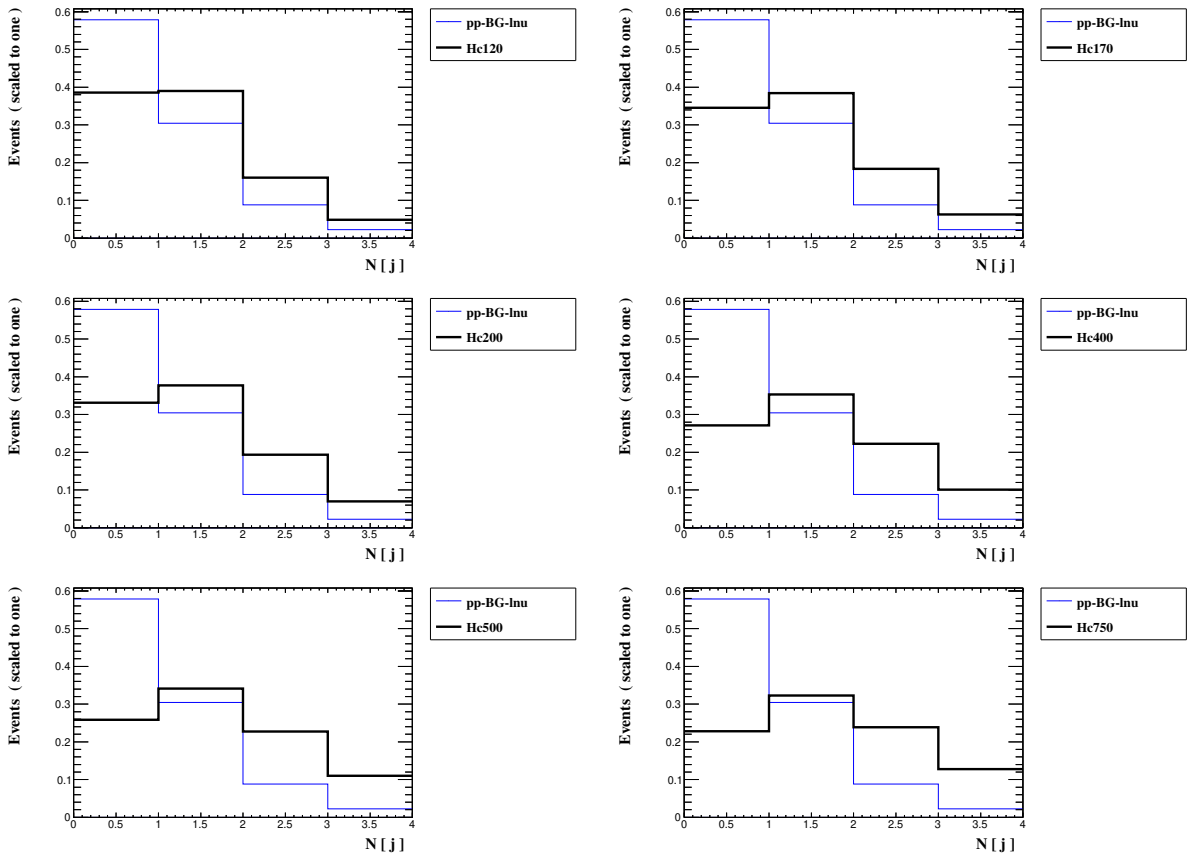


Figure 4.4: Hadron multiplicity plots for signal and background, for selected $M_{H^{\pm}}$ choices of the former, over the acceptance region for leptons and jets, in both transverse momentum and pseudorapidity.

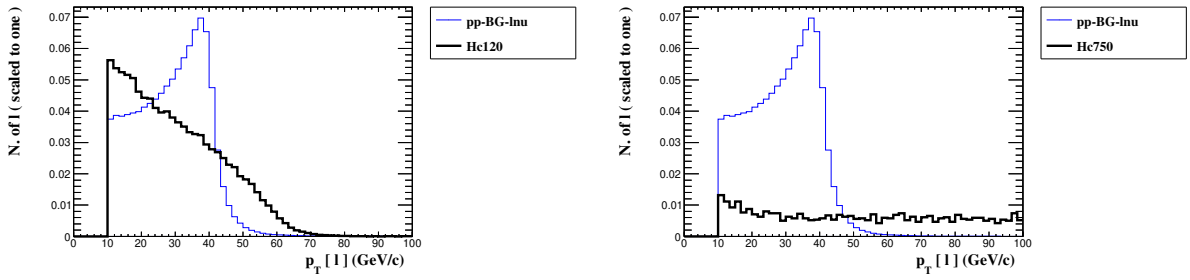


Figure 4.5: Leptonic transverse momentum plots for signal and background, for selected $M_{H^{\pm}}$ choices of the former, over the acceptance region for leptons and jets, in both transverse momentum as pseudorapidity. Further, jets are vetoed here.

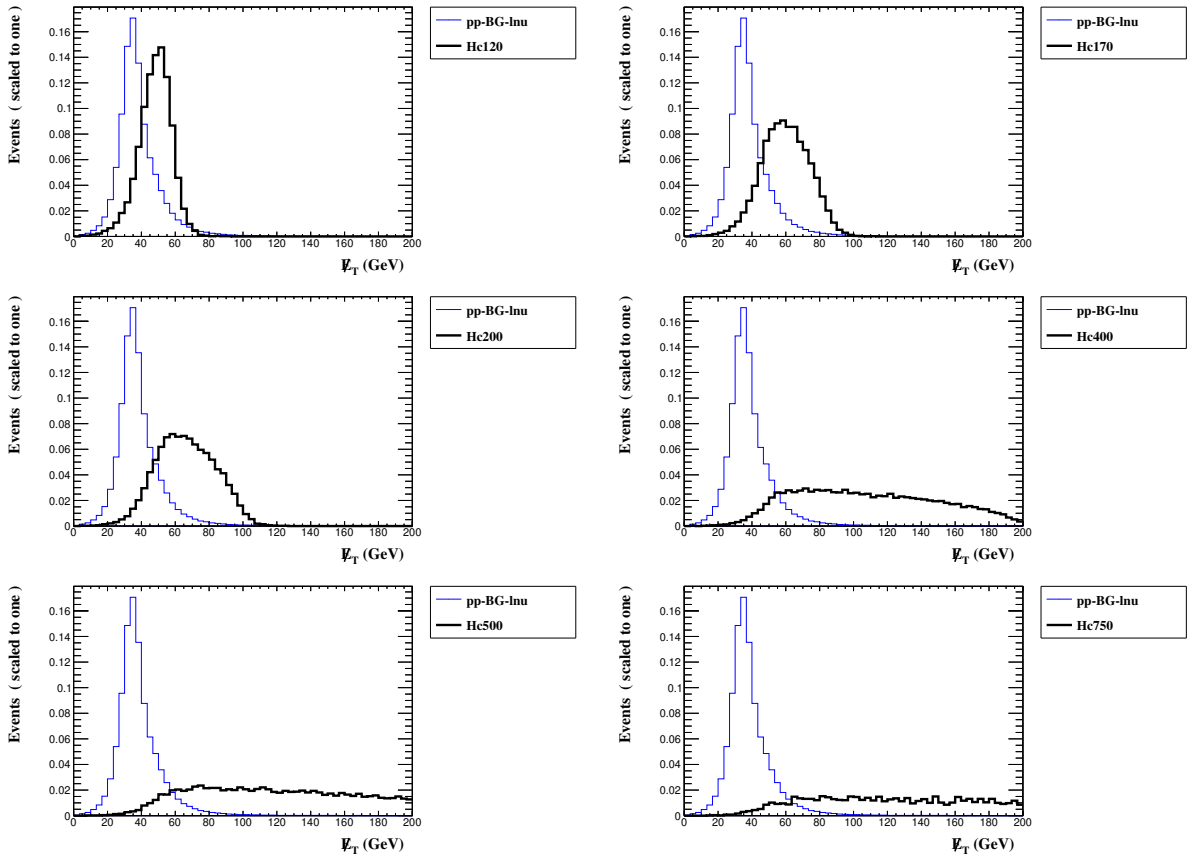


Figure 4.6: Missing transverse energy plots for signal and background, for selected $M_{H^{\pm}}$ choices of the former, over the acceptance region for leptons and jets, in both transverse momentum as pseudorapidity. Further, jets are vetoed here.

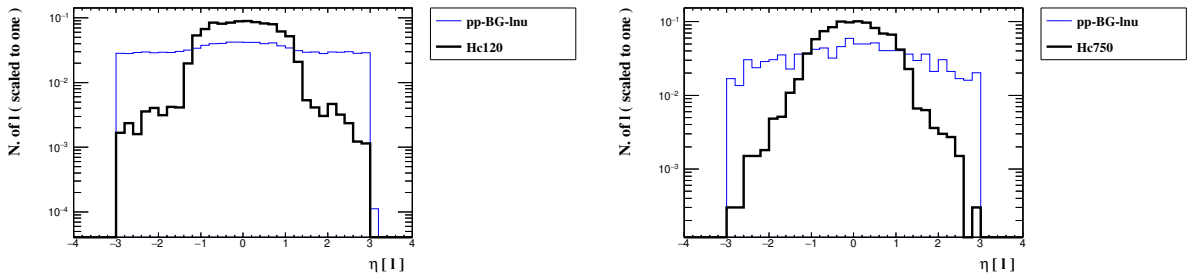


Figure 4.7: Pseudorapidity plots for signal and background, for selected $M_{H^{\pm}}$ choices of the former, over the acceptance region for leptons and jets, in both transverse momentum as pseudorapidity. Further, jets are vetoed here.

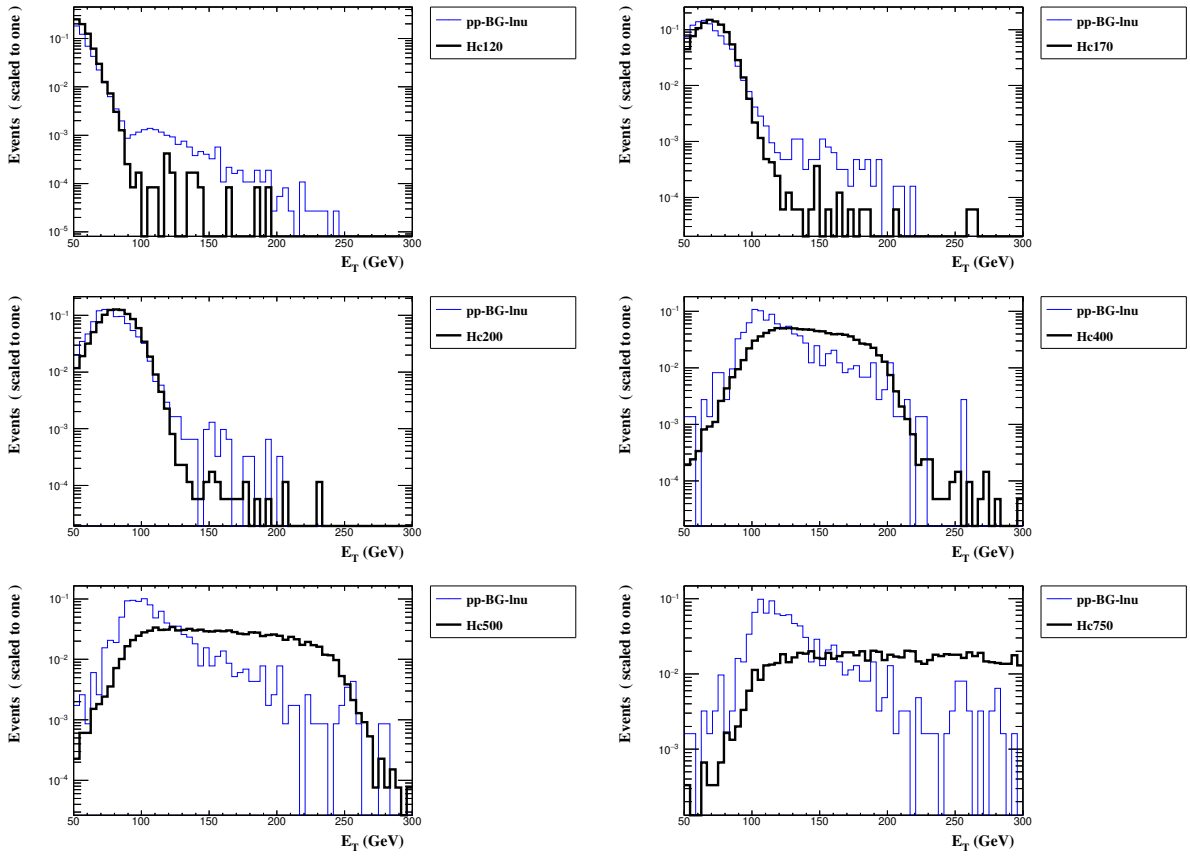


Figure 4.8: Missing transverse energy plots for signal and background, for selected $M_{H^{\pm}}$ choices of the former, over the acceptance region for leptons and jets, in both transverse momentum as pseudorapidity. Further, jets are vetoed here.

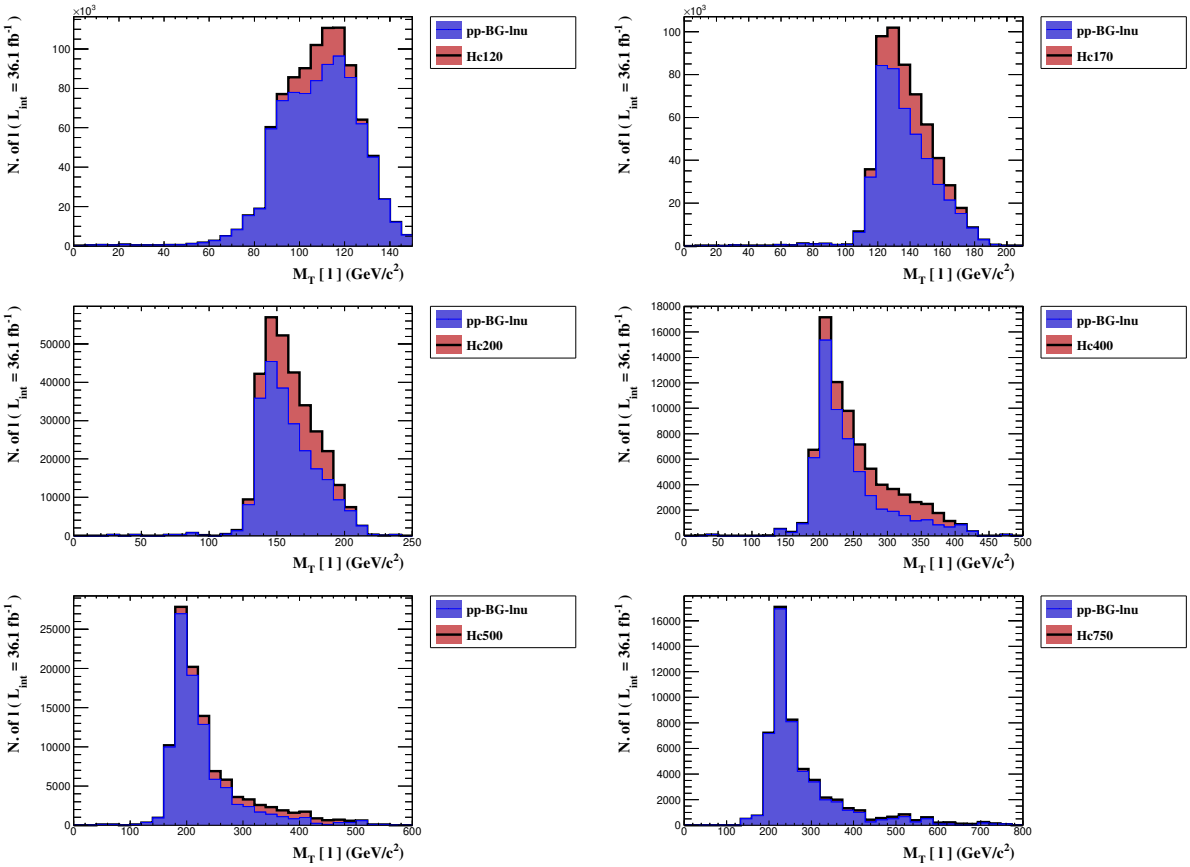


Figure 4.9: Transverse mass plots for signal and background, for selected $M_{H^{\pm}}$ choices of the former, after Cuts 1–4. Histograms are stacked here.

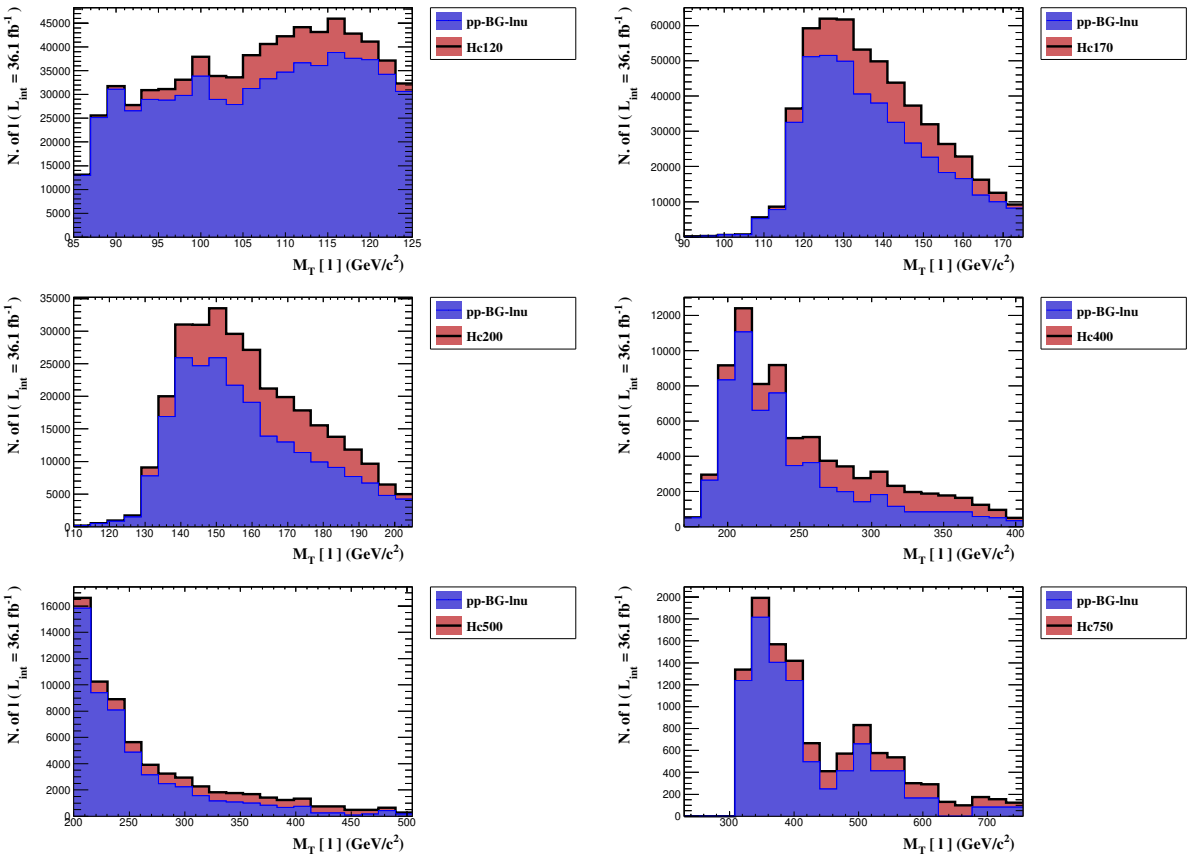


Figure 4.10: Transverse mass plots for signal and background with all cuts taken into account, i.e., limited to the region used for the calculation of the significances.

# Chapter 5

# Conclusions

The potential of a possible future LHeC is assessed, obtained from crossing $e^-$ and $p$ beams in the CERN tunnel currently hosting the LHC and previously LEP. The foreseen beam energies are 60 GeV for the electron and 7 TeV for the proton. Such an environment is rather clean and, since it primarily relies on a charged $W^-$ current for the hard scattering, conducive to the production of a negatively charged Higgs boson, $H^-$. This state is typical of 2HDMs and it is notoriously elusive at the LHC [44, 20], so that it is natural to assess the scope for its detection at the LHeC. As 2HDM theoretical framework it has been adopted a 2HDM-III supplemented by a four-zero-texture in the Yukawa sector which enables one, firstly, to avoid imposing a $Z_2$ symmetry to prevent FCNCs and, secondly, to re-create the standard 2HDM setups, known as Type I, II, X and Y, through suitable choices of the texture matrix elements. Such a scenario can realistically only afford one with LHeC sensitivity to rather light $H^\pm$ masses, i.e., well below the top mass. In this mass regime, though, it is established that the LHeC can access $H^\pm$ masses up to 130 GeV or so, for luminosity conditions already foreseen for such a machine. This assessment is essentially similar for all 2HDM-III incarnations, although sensitivity is primarily established in the like-I, -II and -Y cases via $H^- \to b\bar{c}$ and in the like-X case via $H^- \to \tau\bar{\nu}_\tau$ (assuming electron/muon decays of the $\tau$). The LHeC production mode is $e^-q \to \nu_e H^- q$, with $q = b$ being the dominant sub-channel, the latter being also induced by neutral Higgs boson exchange in $t$-channel (see Fig. 3.1). Hence, on the one hand, one can exploit the very efficient $b$-tagging expected at the LHeC detectors in order to establish the two signals above and beyond a variety of background channels.

On the other hand, heavier $H^\pm$ masses can be studied at the LHC, yet the background noise makes it difficult to be seen. In this thesis a good scenario, yet very constrained, is proposed to be studied in the cleanest channel possible: the $H^\pm \to \tau\nu_\tau$ decay. Also the adopted 2HDM-III supplemented by a four-zero-texture have not enough events in the cases of the like-I, -II and -Y cases via $H^\pm \to cb$, being only the like-X scenario the one with enough events. Further study shall proceed after this thesis is presented.

# Appendix A

# Bash programs to compute the Benchmark Points, Branching Ratios and Cross Sections.

The computation of the benchmark points is done by using a $C++$ program. In this program, the precision, $\lambda_{ij}$ parameters and the Higgs bosons masses can be set, also it computes the contraints given by theoretical and experimental results. A bash program was built in order to acquire the benchmark points:

```
g++ -o BR-Y Branching-Ratio.cpp
g++ -o sigma-Y Cross-section.cpp
./BR-Y thdm X 0 60 Yc -10 60 Y
./sigma-Y thdm X 0 60 Yc -10 60 Y
```

after having the benchmark points, a second bash was built, which computes through CalcHEP the branching ratios and cross section for a given case and saves them in separate files. The bash for the branching ratio is written as follows:

```
#!/usr/bin/env bash
#
# Cambiar al directori de trabajo de Calchep.
cd ~/CalcHEP/calchep_3.6.29/2HDM-III_BR_Hc-I-Y/results/

for(( COUNTER=1; COUNTER<=211;COUNTER++))
do
    echo El contador es $COUNTER

# Copiar c/u de los Benchmarks points al directorio de trabajo
# en un archivo de nombre fort.batch o cualquier otro.
    cp ~/2HDM-Programas/2HDM-BR-sigma-Hc_110GeV-HH_150GeV-HA_100GeV_Constrained/Y-scenario/thdm-YBR_$COUNTER.dat fo


# La salida de la ejecucion de fort.batch pasarla a un archivo outnew1.dat
    ./fort.batch > exitFort.dat

# Cada salida copiarla a un archivo distinto cross_$COUNTER.out
    cp exitFort.dat ~/2HDM-Programas/2HDM-BR-sigma-Hc_110GeV-HH_150GeV-HA_100GeV_Constrained/Y-scenario/BR/BR-Y_$CO

# Las salidas de cada uno reunirlas en un solo archivo outall1.dat
    cat exitFort.dat >> BRT-Y.dat

done
```

while the cross section one as:

## APPENDIX A. BASH PROGRAMS TO COMPUTE THE BENCHMARK POINTS, BRANCHING RATIOS AND CROSS SECTIONS.

```
#!/usr/bin/env bash
#
# Cambiar al directori de trabajo de Calchep.
cd ~/CalcHEP/calchep_3.6.29/2HDM_ep-nuHcq-I-Y/results/

for(( COUNTER=1; COUNTER<=211;COUNTER++))
do
    echo El contador es $COUNTER

# Copiar c/u de los Benchmarks points al directorio de trabajo
# en un archivo de nombre fort.batch o cualquier otro.
    cp ~/2HDM-Programas/2HDM-BR-sigma-Hc_110GeV-HH_150GeV-HA_100GeV_Constrained/Y-scenario/thdm-Ysig_$COUNTER.dat f


# La salida de la ejecucion de fort.batch pasarla a un archivo outnew1.dat
    ./fort.batch > exitFort.dat

# Cada salida copiarla a un archivo distinto cross_$COUNTER.out
    cp exitFort.dat ~/2HDM-Programas/2HDM-BR-sigma-Hc_110GeV-HH_150GeV-HA_100GeV_Constrained/Y-scenario/sigma_ep-nu

# Las salidas de cada uno reunirlas en un solo archivo outall1.dat
    cat exitFort.dat >> sigmaT-Y.dat

done
```

Here both cases are done for the scenario-Y. Depending on what scenario is wished for, a CalcHEP folder with the proper scenario should be done and called in the bash.

After all this, a last bash program is run to acquire the desired data from the generated files, and write these data in a format that Mathematica is capable of plotting:

```
g++ -std=c++11 -o lee_ep-nuhcq-Y lee5files.cpp
./lee_ep-nuhcq-Y XYc-Y.txt cross_ep-nuhcq-Y.txt bran-Y.txt forMath_ep-nuhcq-Y
```

This methology is the same to acquire the standard model background.

# Appendix B

# Pythia Cards.

For the case of the LHeC, the MSTP(11) has to be changed to be = 0. This is explained in the Pythia 6.4 manual [91], as follows:

> "*MSTP(11): (D = 1) use of electron parton distribution in $e^+e^-$ and ep interactions. = 0 : no, i.e. electron carries the whole beam energy. = 1 : yes, i.e. electron carries only a fraction of beam energy in agreement with next-to-leading electron parton-distribution function, thereby including the effects of initial-state bremsstrahlung*".

If this switch is not changed to zero, then the simulation is simply not possible. The cards used in this work were

```
! Read a SLHA file grenerated by CalcHep, this file has information about spectrim and decay table.
IMSS(1)=1
IMSS(13)=1
! Read-in the spectrum SLHA file for decay
IMSS(21)=1
IMSS(22)>0
!Check possible errors during program execution, 0 not check, 1 check but continued (until 10), 2 check and stop
MSTU(21)=0
MSTP(11)=0
! this is the MadGraph Card
!...Parton showering on or off

      MSTP(61)=1
      MSTP(71)=1

!...Fragmentation/hadronization on or off

      PARU(52)=5 !
      PARU(51)=2.5 ! eta
      PARU(53)=15 ! energa transversa mnima del jet
      PARU(54)=0.5 ! Delta(R) del cono
      MSTJ(1)=1

!...Multiple interactions on or off
!      MSTP(81)=20

!...PDFset if MG set not supported by pythia-pgs package (set in lhapdf5 or higher)
!      LHAID= 10041

!LHAPATH=$HOME/HEP/MG5_aMC_v2_3_3/pythia-pgs/src/PDFsets
```

# Bibliography


[1] M. Aaboud et al. Searches for the $Z\gamma$ decay mode of the Higgs boson and for new high-mass resonances in $pp$ collisions at $\sqrt{s} = 13$ TeV with the ATLAS detector. *JHEP*, 10:112, 2017.

[2] M. Aaboud et al. Combined measurement of differential and total cross sections in the $H \to \gamma\gamma$ and the $H \to ZZ^* \to 4\ell$ decay channels at $\sqrt{s} = 13$ TeV with the ATLAS detector. *Phys. Lett.*, B786:114–133, 2018.

[3] Morad Aaboud et al. Measurement of the Higgs boson mass in the $H \to ZZ^* \to 4\ell$ and $H \to \gamma\gamma$ channels with $\sqrt{s} = 13$ TeV $pp$ collisions using the ATLAS detector. *Phys. Lett.*, B784:345–366, 2018.

[4] Georges Aad et al. Observation of a new particle in the search for the Standard Model Higgs boson with the ATLAS detector at the LHC. *Phys.Lett.*, B716:1–29, 2012.

[5] Georges Aad et al. Measurements of the Higgs boson production and decay rates and constraints on its couplings from a combined ATLAS and CMS analysis of the LHC pp collision data at $\sqrt{s} = 7$ and 8 TeV. *JHEP*, 08:045, 2016.

[6] T. Aaltonen et al. Search for Higgs Bosons Produced in Association with $b$-quarks. *Phys. Rev.*, D85:032005, 2012.

[7] V. M. Abazov et al. Search for Charged Higgs Bosons in Top Quark Decays. *Phys. Lett.*, B682:278–286, 2009.

[8] Victor Mukhamedovich Abazov et al. Search for Neutral Higgs Bosons in the Multi-$b$-Jet Topology in 5.2fb$^{-1}$ of $p\bar{p}$ Collisions at $\sqrt{s} = 1.96$ TeV. *Phys. Lett.*, B698:97–104, 2011.

[9] B. Abbott et al. Search for charged higgs bosons in decays of top quark pairs. *Phys. Rev. Lett.*, 82:4975–4980, 1999.

[10] A. Abulencia et al. Search for charged Higgs bosons from top quark decays in $p\bar{p}$ collisions at $\sqrt{s} = 1.96$-TeV. *Phys. Rev. Lett.*, 96:042003, 2006.

[11] A. Airapetian et al. ATLAS: Detector and physics performance technical design report. Volume 2. 1999.

[12] I. J. R. Aitchison and A. J. G. Hey. *Gauge Theories in Particle Physics: A Practical Introduction. Vol. 1: From Relativistic Quantum Mechanics to QED*. IOP, 2003.

[13] A. G. Akeroyd. Nonminimal neutral Higgs bosons at LEP-2. *Phys. Lett.*, B377:95–101, 1996.

[14] A. G. Akeroyd, S. Moretti, and J. Hernandez-Sanchez. Light charged Higgs bosons decaying to charm and bottom quarks in models with two or more Higgs doublets. *Phys. Rev.*, D85:115002, 2012.

[15] A. G. Akeroyd and W. James Stirling. Light charged Higgs scalars at high-energy e+ e- colliders. *Nucl. Phys.*, B447:3–17, 1995.

[16] J R Andersen et al. Handbook of LHC Higgs Cross Sections: 3. Higgs Properties. 2013.

[17] Mayumi Aoki, Shinya Kanemura, Koji Tsumura, and Kei Yagyu. Models of Yukawa interaction in the two Higgs doublet model, and their collider phenomenology. *Phys. Rev.*, D80:015017, 2009.

[18] Alfredo Aranda, Cesar Bonilla, and J. Lorenzo Diaz-Cruz. Three generations of Higgses and the cyclic groups. *Phys. Lett.*, B717:248–251, 2012.

[19] Alfredo Aranda, Cesar Bonilla, Raymundo Ramos, and Alma D. Rojas. Model of flavor with quaternion symmetry. *Phys. Rev.*, D84:016009, 2011.

[20] A. Arhrib, R. Benbrik, H. Harouiz, S. Moretti, and A. Rouchad. *A Guidebook to Hunting Charged Higgs Bosons at the LHC*.

[21] R. Barate et al. Search for the standard model Higgs boson at LEP. *Phys. Lett.*, B565:61–75, 2003.

[22] J. E. Barradas Guevara, F. C. Cazarez Bush, A. Cordero Cid, O. Felix Beltran, J. Hernandez Sanchez, and R. Noriega Papaqui. Implications of Yukawa Textures in the decay $H^+ \to W^+\gamma$ within the 2HDM-III. *J. Phys.*, G37:115008, 2010.

[23] A. Belyaev, N. D. Christensen, and A. Pukhov. *CalcHEP 3.4 for collider physics within and beyond the Standard Model.*

[24] Johan Bijnens, Jie Lu, and Johan Rathsman. Constraining General Two Higgs Doublet Models by the Evolution of Yukawa Couplings. *JHEP*, 05:118, 2012.

[25] Francesca Borzumati and Christoph Greub. 2HDMs predictions for anti-B —¿ X(s) gamma in NLO QCD. *Phys. Rev.*, D58:074004, 1998.

[26] Francesca Borzumati and Christoph Greub. Two Higgs doublet model predictions for anti-B —¿ X(s) gamma in NLO QCD: Addendum. *Phys. Rev.*, D59:057501, 1999.

[27] G. C. Branco, D. Emmanuel-Costa, and C. Simoes. Nearest-Neighbour Interaction from an Abelian Symmetry and Deviations from Hermiticity. *Phys. Lett.*, B690:62–67, 2010.

[28] Marcela S. Carena, Peter M. Zerwas, E. Accomando, P. Bagnaia, A. Ballestrero, et al. Higgs physics at LEP-2. 1996.

[29] S. Catani, M. Dittmar, J. Huston, D.E. Soper, S. Tapprogge, et al. The QCD and standard model working group: Summary report. 2000.

[30] S. Catani, M. Dittmar, D.E. Soper, W. James Stirling, S. Tapprogge, et al. QCD. 2000.

[31] Serguei Chatrchyan et al. Searches for Higgs Bosons in pp Collisions at $\sqrt{s} = 7$ and 8 TeV in the Context of Four-Generation and Fermiophobic Models. *Phys. Lett.*, B725:36–59, 2013.

[32] CMS Collaboration. Properties of the observed Higgs-like resonance using the diphoton channel. 2013.

[33] CMS Collaboration. Search for new resonances in the diphoton final state in the mass range between 70 and 110 GeV in pp collisions at $\sqrt{s} = 8$ and 13 TeV. 2017.

[34] E. Conte, B. Fuks, and G. Serret. Madanalysis 5, a user-friendly framework for collider phenomenology. *Comput. Phys. Commun.* **184**, *222 (2013).*

[35] J. Conway, R. Culbertson, R. Demina, B. Kilminster, M. Kruse, S. Mrenna, J. Nielsen, M. Roco, A. Pierce, J. Thaler, and T. Wizansky.

[36] Andreas Crivellin, Ahmet Kokulu, and Christoph Greub. Flavor-phenomenology of two-Higgs-doublet models with generic Yukawa structure. *Phys. Rev.*, D87(9):094031, 2013.

[37] S. P. Das, J. Hernandez-Sanchez, S. Moretti, A. Rosado, and R. Xoxocotzi. Flavor violating signatures of lighter and heavier higgs bosons within the two higgs doublet model type-iii at the lhec. *Phys. Rev. D* **94**, *no. 5, 055003 (2016).*

[38] S. Dawson. Introduction to the physics of Higgs bosons. 1994.

[39] S. Dawson. Introduction to electroweak symmetry breaking. pages 1–83, 1998.

[40] N. G. Deshpande and E. Ma. Pattern of symmetry breaking with two higgs doublets. *Phys. Rev. D* **18**, *2574 (1978).*

[41] J. L. Diaz-Cruz, J. Hernandez-Sanchez, S. Moretti, R. Noriega-Papaqui, and A. Rosado. Yukawa textures and charged higgs boson phenomenology in the 2hdm-iii. *Phys. Rev. D* **79**, *095025 (2009).*

[42] J. L. Diaz-Cruz and A. Mendez. Vacuum alignment in multiscalar models. *Nucl. Phys. B* **380**, *39 (1992).*

[43] J. L. Diaz-Cruz, R. Noriega-Papaqui, and A. Rosado. Measuring the fermionic couplings of the Higgs boson at future colliders as a probe of a non-minimal flavor structure. *Phys. Rev.*, D71:015014, 2005.

[44] A. G. Akeroyd *et al.* Prospects for charged higgs searches at the lhc. *Eur. Phys. J. C* **77**, *no. 5, 276 (2017).*

[45] E. Accomando *et al.* Workshop on cp studies and non-standard higgs physics.

[46] V. Fanti *et al.* [NA48 Collaboration]. A new measurement of direct cp violation in two pion decays of the neutral kaon. *Phys. Lett. B* **465**, *335 (1999).*

[47] O. Felix-Beltran, F. Gonzalez-Canales, J. Hernandez-Sanchez, S. Moretti, R. Noriega-Papaqui, and A. Rosado. Analysis of the quark sector in the 2hdm with a four-zero yukawa texture using the most recent data on the ckm matrix. *Phys. Lett. B* **742**, *347 (2015).*

[48] R.P. Feynman and Murray Gell-Mann. Theory of Fermi interaction. *Phys.Rev.*, 109:193–198, 1958.

[49] Paul H. Frampton and Shinya Matsuzaki. Renormalizable A(4) Model for Lepton Sector. 2008.

[50] Michele Frigerio, Satoru Kaneko, Ernest Ma, and Morimitsu Tanimoto. Quaternion family symmetry of quarks and leptons. *Phys. Rev.*, D71:011901, 2005.

[51] H. Fritzsch and Z. z. Xing. Four zero texture of hermitian quark mass matrices and current experimental tests. *Phys. Lett. B* **555**, *63 (2003).*

[52] Takeshi Fukuyama, Hiroaki Sugiyama, and Koji Tsumura. Phenomenology in the Higgs Triplet Model With the $A_4$ Symmetry. *Phys. Rev.*, D82:036004, 2010.

[53] L. Lavoura M. N. Rebelo M. Sher G. C. Branco, P. M. Ferreira and J. P. Silva. Theory and phenomenology of two-higgs-doublet models. *Phys. Rept.* **516**, *1 (2012)*.

[54] Murray Gell-Mann. A schematic model of baryons and mesons. *Phys. Lett.*, 8:214–215, 1964.

[55] I. F. Ginzburg and M. Krawczyk. Symmetries of two higgs doublet model and cp violation. *Phys. Rev. D* **72**, *115013 (2005)*.

[56] S. L. Glashow and S. Weinberg. Natural conservation laws for neutral currents. *Phys. Rev. D* **15**, *1958 (1977)*.

[57] Sheldon L. Glashow. Partial-symmetries of weak interactions. *Nuclear Physics*, 22(4):579 – 588, 1961.

[58] J. Goldstone. Field Theories with Superconductor Solutions. *Nuovo Cim.*, 19:154–164, 1961.

[59] Jeffrey Goldstone, Abdus Salam, and Steven Weinberg. Broken Symmetries. *Phys.Rev.*, 127:965–970, 1962.

[60] M. Gomez-Bock and R. Noriega-Papaqui. Flavor violating decays of the Higgs bosons in the THDM-III. *J. Phys.*, G32:761–776, 2006.

[61] D. Griffiths. *Introduction to Elementary Particles*. Wiley-VCH, 2004.

[62] Yuval Grossman. Phenomenology of models with more than two Higgs doublets. *Nucl. Phys.*, B426:355–384, 1994.

[63] John F. Gunion, Howard E. Haber, Gordon L. Kane, and Sally Dawson. The Higgs Hunter's Guide. *Front.Phys.*, 80:1–448, 2000.

[64] H. E. Haber. In *Testing the Standard Model*, pages 340–475. Proceedings of the 1990 Theoretical Advanced Study Institute in Elementary Particle Physics edited by M. Cvetic and P. Langacker (World Scientific, Singapore, 1991), 1991.

[65] J. Hernandez-Sanchez, C. G. Honorato, M. A. Perez, and J. J. Toscano. The $\gamma\gamma \to \phi_i\phi_j$ processes in the type-III two-Higgs-doublet model. *Phys. Rev.*, D85:015020, 2012.

[66] J. Hernandez-Sanchez, S. Moretti, R. Noriega-Papaqui, and A. Rosado. Off-diagonal terms in yukawa textures of the type-iii 2-higgs doublet model and light charged higgs boson phenomenology. *JHEP* **1307**, *044 (2013)*.

[67] M. Herrero. The Standard model. *NATO Sci.Ser.C*, 534:1–59, 1999.

[68] Peter W. Higgs. Broken symmetries and the masses of gauge bosons. *Phys. Rev. Lett.*, 13:508–509, Oct 1964.

[69] Peter W. Higgs. Spontaneous symmetry breakdown without massless bosons. *Phys. Rev.*, 145:1156–1163, May 1966.

[70] Martin Jung, Antonio Pich, and Paula Tuzon. Charged-Higgs phenomenology in the Aligned two-Higgs-doublet model. *JHEP*, 11:003, 2010.

[71] M. M. Kado and C. G. Tully. The searches for Higgs bosons at LEP. *Ann. Rev. Nucl. Part. Sci.*, 52:65–113, 2002.

[72] Gordon Kane. *Modern Elementary Particle Physics*. 1988.

[73] Maria Krawczyk and David Temes. 2HDM(II) radiative corrections in leptonic tau decays. *Eur. Phys. J.*, C44:435–446, 2005.

[74] T. D. Lee. Cp nonconservation and spontaneous symmetry breaking. *Phys. Rept.* **9**, *143 (1974)*.

[75] T. D. Lee. A theory of spontaneous t violation. *Phys. Rev. D* **8**, *1226 (1973)*.

[76] J. Liu and L. Wolfenstein. Spontaneous cp violation in the su(2)-l x u(1)-y model with two higgs doublets. *Nucl. Phys. B* **289**, *1 (1987)*.

[77] Heather E. Logan and Deanna MacLennan. Charged Higgs phenomenology in the lepton-specific two Higgs doublet model. *Phys. Rev.*, D79:115022, 2009.

[78] Farvah Mahmoudi and Oscar Stal. Flavor constraints on the two-Higgs-doublet model with general Yukawa couplings. *Phys. Rev.*, D81:035016, 2010.

[79] K.A. Olive and Particle Data Group. Review of particle physics. *Chinese Physics C*, 38(9):090001, 2014.

[80] Antonio Pich and Paula Tuzon. Yukawa Alignment in the Two-Higgs-Doublet Model. *Phys. Rev.*, D80:091702, 2009.

[81] J. Pumplin, D. R. Stump, J. Huston, H. L. Lai, P. M. Nadolsky, and W. K. Tung. New generation of parton distributions with uncertainties from global qcd analysis. *JHEP* **0207**, *012 (2002)*.

[82] Chris Quigg. The Electroweak theory. pages 3–67, 2002.

[83] R. G. Roberts, A. Romanino, Graham G. Ross, and L. Velasco-Sevilla. Precision Test of a Fermion Mass Texture. *Nucl. Phys.*, B615:358–384, 2001.

[84] Lewis H. Ryder. *Quantum Field Theory*. Cambridge University Press, 2 edition, June 1996.

[85] S. Schael et al. Search for neutral MSSM Higgs bosons at LEP. *Eur. Phys. J.*, C47:547–587, 2006.

[86] Albert M Sirunyan et al. Search for a charged Higgs boson decaying to charm and bottom quarks in proton-proton collisions at $\sqrt{s} = 8$ TeV. *JHEP*, 11:115, 2018.

[87] Albert M. Sirunyan et al. Search for the decay of a Higgs boson in the $\ell\ell\gamma$ channel in proton-proton collisions at $\sqrt{s} = 13$ TeV. *JHEP*, 11:152, 2018.

[88] Albert M Sirunyan et al. Combined measurements of Higgs boson couplings in protonproton collisions at $\sqrt{s} = 13\,\text{TeV}$. *Eur. Phys. J.*, C79(5):421, 2019.

[89] Albert M Sirunyan et al. Search for a heavy pseudoscalar boson decaying to a Z and a Higgs boson at $\sqrt{s} =$ 13 TeV. *Eur. Phys. J.*, C79(7):564, 2019.

[90] Albert M Sirunyan et al. Search for charged Higgs bosons in the $\text{H}^{\pm} \to \tau^{\pm}\nu_{\tau}$ decay channel in proton-proton collisions at $\sqrt{s} = 13$ TeV. *JHEP*, 07:142, 2019.

[91] Torbjorn Sjostrand, Stephen Mrenna, and Peter Z. Skands. PYTHIA 6.4 Physics and Manual. *JHEP*, 05:026, 2006.

[92] M. Tanabashi, K. Hagiwara, K. Hikasa, K. Nakamura, Y. Sumino, F. Takahashi, J. Tanaka, K. Agashe, G. Aielli, C. Amsler, M. Antonelli, D. M. Asner, H. Baer, Sw. Banerjee, R. M. Barnett, T. Basaglia, C. W. Bauer, J. J. Beatty, V. I. Belousov, J. Beringer, S. Bethke, A. Bettini, H. Bichsel, O. Biebel, K. M. Black, E. Blucher, O. Buchmuller, V. Burkert, M. A. Bychkov, R. N. Cahn, M. Carena, A. Ceccucci, A. Cerri, D. Chakraborty, M.-C. Chen, R. S. Chivukula, G. Cowan, O. Dahl, G. D'Ambrosio, T. Damour, D. de Florian, A. de Gouvêa, T. DeGrand, P. de Jong, G. Dissertori, B. A. Dobrescu, M. D'Onofrio, M. Doser, M. Drees, H. K. Dreiner, D. A. Dwyer, P. Eerola, S. Eidelman, J. Ellis, J. Erler, V. V. Ezhela, W. Fetscher, B. D. Fields, R. Firestone, B. Foster, A. Freitas, H. Gallagher, L. Garren, H.-J. Gerber, G. Gerbier, T. Gershon, Y. Gershtein, T. Gherghetta, A. A. Godizov, M. Goodman, C. Grab, A. V. Gritsan, C. Grojean, D. E. Groom, M. Grünewald, A. Gurtu, T. Gutsche, H. E. Haber, C. Hanhart, S. Hashimoto, Y. Hayato, K. G. Hayes, A. Hebecker, S. Heinemeyer, B. Heltsley, J. J. Hernández-Rey, J. Hisano, A. Höcker, J. Holder, A. Holtkamp, T. Hyodo, K. D. Irwin, K. F. Johnson, M. Kado, M. Karliner, U. F. Katz, S. R. Klein, E. Klempt, R. V. Kowalewski, F. Krauss, M. Kreps, B. Krusche, Yu. V. Kuyanov, Y. Kwon, O. Lahav, J. Laiho, J. Lesgourgues, A. Liddle, Z. Ligeti, C.-J. Lin, C. Lippmann, T. M. Liss, L. Littenberg, K. S. Lugovsky, S. B. Lugovsky, A. Lusiani, Y. Makida, F. Maltoni, T. Mannel, A. V. Manohar, W. J. Marciano, A. D. Martin, A. Masoni, J. Matthews, U.-G. Meißner, D. Milstead, R. E. Mitchell, K. Mönig, P. Molaro, F. Moortgat, M. Moskovic, H. Murayama, M. Narain, P. Nason, S. Navas, M. Neubert, P. Nevski, Y. Nir, K. A. Olive, S. Pagan Griso, J. Parsons, C. Patrignani, J. A. Peacock, M. Pennington, S. T. Petcov, V. A. Petrov, E. Pianori, A. Piepke, A. Pomarol, A. Quadt, J. Rademacker, G. Raffelt, B. N. Ratcliff, P. Richardson, A. Ringwald, S. Roesler, S. Rolli, A. Romaniouk, L. J. Rosenberg, J. L. Rosner, G. Rybka, R. A. Ryutin, C. T. Sachrajda, Y. Sakai, G. P. Salam, S. Sarkar, F. Sauli, O. Schneider, K. Scholberg, A. J. Schwartz, D. Scott, V. Sharma, S. R. Sharpe, T. Shutt, M. Silari, T. Sjöstrand, P. Skands, T. Skwarnicki, J. G. Smith, G. F. Smoot, S. Spanier, H. Spieler, C. Spiering, A. Stahl, S. L. Stone, T. Sumiyoshi, M. J. Syphers, K. Terashi, J. Terning, U. Thoma, R. S. Thorne, L. Tiator, M. Titov, N. P. Tkachenko, N. A. Törnqvist, D. R. Tovey, G. Valencia, R. Van de Water, N. Varelas, G. Venanzoni, L. Verde, M. G. Vincter, P. Vogel, A. Vogt, S. P. Wakely, W. Walkowiak, C. W. Walter, D. Wands, D. R. Ward, M. O. Wascko, G. Weiglein, D. H. Weinberg, E. J. Weinberg, M. White, L. R. Wiencke, S. Willocq, C. G. Wohl, J. Womersley, C. L. Woody, R. L. Workman, W.-M. Yao, G. P. Zeller, O. V. Zenin, R.-Y. Zhu, S.-L. Zhu, F. Zimmermann, P. A. Zyla, J. Anderson, L. Fuller, V. S. Lugovsky, and P. Schaffner. Review of particle physics. *Phys. Rev. D*, 98:030001, Aug 2018.

[93] Michael Trott and Mark B. Wise. On Theories of Enhanced CP Violation in $B_{s,d}$ Meson Mixing. *JHEP*, 11:157, 2010.

[94] M. H. G. Tytgat. The inert doublet model: A new archetype of wimp dark matter? *J. Phys. Conf. Ser.* **120**, *042026 (2008).*

[95] S. Weinberg. Gauge theory of cp violation. *Phys. Rev. Lett.* **37**, *657 (1976).*

[96] Steven Weinberg. A Model of Leptons. *Phys.Rev.Lett.*, 19:1264–1266, 1967.

[97] Y. L. Wu and L. Wolfenstein. Sources of cp violation in the two higgs doublet model. *Phys. Rev. Lett.* **73**, *1762 (1994).*

[98] Zhen-jun Xiao and Libo Guo. B0 anti-B0 mixing and B —¿ X(s) gamma decay in the third type 2HDM: Effects of NLO QCD contributions. *Phys. Rev.*, D69:014002, 2004.